PHYSICAL REVIEW C **75**, 064313 (2007)

Scission configurations and their implication in fission-fragment angular momenta

L. Bonneau,[1,2] P. Quentin,[1,2] and I. N. Mikhailov[3,4]
[1] *Theoretical Division, Los Alamos National Laboratory, Los Alamos, New Mexico 87545, USA*
[2] *Université Bordeaux 1, CNRS/IN2P3, Centre d'Etudes Nucléaires de Bordeaux-Gradignan, UMR 5797, Chemin du Solarium, BP 120, F-33175 Gradignan, France*
[3] *Bogoliubov Laboratory of Theoretical Physics, JINR, RU-141980 Dubna, Moscow region, Russia*
[4] *Centre de Spectrométrie Nucléaire et de Spectrométrie de Masse, CNRS-IN2P3, and Université Paris XI, F-91405 Orsay, France*

(Received 6 February 2007; published 19 June 2007)

The generation of sizable angular momenta in fragments formed in low-energy nuclear fission is described microscopically within the general quantum-mechanical framework of orientation pumping due to the Heisenberg uncertainty principle. Within this framework, we make use of the results of Skyrme-Hartree-Fock plus BCS-pairing calculations of fragment deformabilities to deduce a distribution of fission-fragment spins as a function of the fragment total excitation energy. We consider a fragmentation corresponding to a pair of deformed fragments and for which fission data are available. The properties of the scission configurations determine to a large extent the fission-fragment spins. This is why we pay particular attention to quantitatively defining the scission configurations and to studying the various implications of such a specific choice. A fair qualitative agreement with data is demonstrated and discussed within the limits of the simple scission-configuration model used here.

DOI: 10.1103/PhysRevC.75.064313 PACS number(s): 21.60.Jz, 24.75.+i

I. INTRODUCTION

Fission fragments resulting from the fission at low energy (neutron or light charged particle induced fission) or even zero energy (as in spontaneous fission) end up with angular momenta widely distributed in a range going from typically a few to about $10\hbar$. This result was obtained long ago and further confirmed in a variety of different experimental situations (for reviews and comprehensive references see, e.g., Refs. [1–3]). It was first evidenced by the observation of prompt γ-ray emission by the fragments, where "prompt" here means much before the β decay of the neutron-rich nuclear species produced in the fission of the heavy nuclei under consideration (actinide or beyond). However, the current wisdom is that this γ emission should take place much after the deexcitation by prompt-neutron emission carrying out most of the fragment excitation energy and very little of their angular momenta.

Various theoretical attempts to describe the generation of angular momenta in fission fragments have dwelled on the concept of an excitation at scission of some collective modes capable of producing angular momenta. The rather elusive character of such a specific scission point renders this type of approach as somewhat contingent upon specific assumptions regarding the collective dynamics at this stage of the fission process. The point of this paper is to examine in detail how far basic quantum-mechanical concepts can provide an explanation for most of the experimental facts related to the fission-fragment angular momenta at low excitation energy. In doing so, to be specific, we will at some point have to rely also on a well-defined dynamical assumption for the fission process at scission.

The paper is organized as follows. After a review in Sec. II of the relevant experimental data and, in Sec. III, of the existing theoretical descriptions, we will present in Sec. IV the framework of our approach. Then, Sec. V addresses the concept of scission and provides a quantitative definition. We also specify our model assumptions for the description of the scission configurations. In Sec. VI, we describe how the retained mechanism of angular-momentum generation (proposed by two of us a few years ago [4], briefly reviewed and developed below) has been implemented to calculate the average angular momentum of fission fragments as a function of their total excitation energy. The results obtained for one fragmentation in the ^{252}Cf spontaneous fission, namely, ^{106}Mo+^{146}Ba, are reported and discussed in Sec. VII. The main conclusions of this study are drawn in Sec. VIII.

II. BRIEF SURVEY OF EXPERIMENTAL FINDINGS

The first relevant measurements in, e.g., ^{252}Cf spontaneous fission [5,6] yielded a multiplicity per fission of ten photons having a total energy of 8.6 MeV on average. Later, measurements of angular correlations between the fission fragments and the γ rays (see, e.g., the thermal-neutron fission results of Ref. [7]) exhibited an anisotropy consistent with $E2$ radiation emitted by nuclei rotating with a rotation axis perpendicular to the fragment direction. The γ-emission times are indeed found roughly consistent (see Ref. [8]) with multipolarities being mostly of a dipole and quadrupole character.

The picture which emerged from these global results [9] was that of a γ deexcitation performed by emitting first some statistical $E1$ γ rays until one reaches the yrast line region. Then this dipole emission would be followed by mostly stretched $E2$ γ rays corresponding to transitions within some collective rotational bands in axially deformed fragments. One would get an idea of the spin (in units of $\hbar$) of each fragment by multiplying the measured γ multiplicity by a factor slightly below 2 (taking into account the mostly $E2$ character of the γ rays as exhibited by angular correlation data except for a few $E1$ transitions) and dividing the result by 2 (equally sharing in this crude approach the γ multiplicity between the two fragments). This would lead in ^{252}Cf spontaneous fission to average fragment angular momenta in the $8\hbar$ range.

However, the average energy released by such γ rays has clearly indicated some competition between neutron and γ emissions, If all opportunities to deexcite fragments by neutron emission are taken into account, one would be left with an average total γ energy of the order of the neutron separation energy. For such neutron-rich nuclei, this γ energy would be closer to 5 MeV than to the roughly 8.5 MeV observed for ^{252}Cf.

This competition between the emission of neutrons and γ rays constitutes a first difficulty for the theoretical description of the fragment γ deexcitation, since the observed γ rays do not generally come entirely from the same nucleus. There are, as a matter of fact, some further difficulties in inferring the fragment spins from the data which are mainly related to the wide distribution of γ-emitting nuclear states, even upon fixing their specific nucleonic numbers (N and Z). Indeed, because of the dynamics of the fission process itself (from saddle to scission) as well as the possible prompt-neutron emission processes, one has to deal with a broad distribution of spin and excitation energy before the γ emission, which is rather poorly known.

At this point, it is important to underscore a genuine source of ambiguity in interpreting dynamically the results obtained from fission-fragment spin data. This ambiguity arises from the difference between the identity of the γ-emitting nuclei (the secondary fragments) and the nuclei produced at scission (the primary ones). Viewed as the interplay between nuclear and Coulomb forces, the dynamics of fission is concerned, before and beyond the scission points, mostly with the primary fragments. Therefore, one faces the extreme difficulty of sorting the various “primary” components out of the γ spectra corresponding to “secondary” emission. This encompasses two different problems. The first one is, as we have seen, that some γ rays are emitted before the last neutron. Therefore some γ rays attributed to a secondary fragment do not originate from that fragment. One may, at first, consider that this problem does not impair our understanding of the deexcitation, since the first (dipole) γ rays are statistical in nature and thus not influenced significantly by the particular structure of the emitting nucleus. The second problem is by far more serious. For a given primary fragmentation, the distribution of the number of emitted neutrons may be quite large, reflecting the broad character of the excitation energy distribution, as already mentioned. One might then wish to pinpoint the excitation energy, for example, by selecting data corresponding to a given total kinetic energy bin. Yet, this would not guarantee an unambiguous determination of the primary fragmentation because the total excitation energy is not uniquely shared between the two fragments, resulting in a distribution or possible energies for each, in addition to the above-advocated neutron-γ competition.[1] As a result, it is impossible to perform a one-to-one correspondence between the secondary γ emission and theoretical scission configurations. It is thus very important to note that any experimental data on primary configurations are not, in fact, free from various stringent model assumptions.

This is the case in the pioneering works attempting to deduce fragment spins from the relative yields of isomeric states in the fragments reached in the fission process. In such approaches, one assumes first for each fragment a theoretical initial Gaussian spin distribution parametrized so as to take into account the fragment moment of inertia $\mathcal{J}$ and a temperature T (both being boldly assumed to represent the wide distribution of deformations and excitation energies of a given fragment). These factors are in fact appearing through their product, usually called B^2, in the width of the spin distribution. This product is proportional to the expectation value of the square of the angular momentum in the considered fragment. Through a combined neutron-γ deexcitation model (similar to what Huizenga and Vandenbosch [10] had proposed) one fits the parameter B^2 so as to have the right ratio of spin populations corresponding to the measured isomeric yield.

Shortly after the beginning of these studies, Wilhelmy and collaborators [11] proposed to replace the input of isomeric ratios by those yielded by the intensity of γ rays in ground-state rotational bands (for even-even nuclei). Such basic ideas were utilized later, taking advantage of the advent over the last two decades of so-called $4\pi\gamma$ multidetector arrays. A first kind of such data corresponds to set-ups of high efficiency but poor energy resolution (the fragment identification, at least their mass split, being obtained through coincidence measurements with fragment detectors). An example of such results may be found in Ref. [12]. The second category of γ multidetector array data has been obtained from high-resolution Germanium detectors as EUROBALL or GAMMASPHERE. For an illustration of such an approach, one may refer to Ref. [13] for the ^{252}Cf spontaneous fission using the GAMMASPHERE array in a preliminary stage with 36 Germanium detectors. By analyzing double-coincidence γ spectra, Ter-Akopian and collaborators were able to provide fission yields [14–16] and deduce from the identification of low-lying decay γ cascades the angular momenta of fission fragments [13] for two different splittings (Mo-Ba and Zr-Ce). The fragment spins were obtained after a secondary-to-primary unfolding process using basically the same model assumptions as given above. The authors of Ref. [13] found that as the number of emitted neutrons $\bar{\nu}$ increases from zero to about 6, the fragment spins rise in the two studied cases from an initial value of about $2\hbar$ to values in the 4–$8\hbar$ range (depending on the specific element).

Note that the first results obtained with the isomeric ratios (see Ref. [2] for references) were at variance with the data deduced from the average γ multiplicity (see, e.g., Ref. [17]). The latter exhibit a sawtooth pattern as a function of the mass of the fragments, reminiscent of what is observed for the average neutron multiplicity (as in, e.g., Ref. [18]) which was not borne out by the data in the former technique. An analysis of some γ-multiplicity data with the deexcitation code used for the isomeric yield data also found no sawtooth behavior [11]. More recently, some refined γ-multiplicity measurements [12] exhibited no (or merely a very attenuated) sawtooth pattern.

One can also mention some specific problems met in the above approaches when relating relevant raw γ data to the spin of the fission fragments. First of all, the assumption of a

---

[1] The authors are indebted to Pr. Friedrich Gönnenwein for patient clarifying remarks on these matters.

single spin distribution may be considered as highly dubious even when used to reach averaged quantities, since it overlooks the fact that one has to consider wide (and possibly made of many components) distributions of configurations and energies experienced at this stage of the fission process even for a given fragmentation. To illustrate this, we may recall the experimental example of bimodal fission for the same fragmentation (in that case symmetrical) presented in Ref. [19]. Next, we may also question the use of a unique distribution of initial spins in the particular context of fragment isomeric states. Indeed, these isomers are of quasiparticle nature, and the corresponding potential-energy landscapes might be vastly different between various such complicated single-particle configurations. This is similar to the old problem encountered in the fission-barrier description (for axially symmetrical deformations) under the name of specialization energy [20] which may vary with the approximately conserved usual quantum number K (see, e.g., Ref. [21]). Moreover, we should add that the rotational properties of such quasiparticle isomers are not, by any means, guaranteed to be similar to those of ground states which exhibit a much simpler single-particle structure. The latter is due, in particular, to the different amount of pairing correlations present in ground and isomeric states. A theoretical description of the spins of these fission-fragment isomers should thus require a specific handling of these particular configurations, which will not be attempted here.

Recent experimental results at the Institut Laue Langevin (ILL) Lohengrin mass spectrometer facility [22] are worth mentioning in this context. They exhibit the relative population, as a function of the total kinetic energy, of two isomeric states (10^+, 2.723 MeV, 3.7 μs, and 7^-, 1.925 MeV, 28 μs) of ^{132}Te yielded by the neutron-induced fission of the ^{240}Pu compound nucleus. Gönnenwein and collaborators [22] draw attention to data pertaining to the so-called cold (i.e., in the absence of any intrinsic excitation) deformed fission, where "deformed" means here that the sum of fragment deformation energies reaches its maximum. The observed drop in the population of high-spin states while nearing this cold deformed fission region is clearly at variance with any explanation involving a correlation between spins and deformations. This seems to be a clean-cut example of a mechanism of angular-momentum generation that cannot be explained by the theoretical approach in its present state, as developed below, which relies on collective rotational motion (see the concluding discussion of Sec. III).

Two other considerations should also be made before concluding this survey of experimental approaches of the fission-fragment spin problem. First, the angular momentum of a fragment is modified when a neutron and/or a statistical γ ray is emitted. Calculations using statistical evaporation codes have shown that on average the spin of the emitting nucleus is modified by $0.5\hbar$ per emitted neutron and $0.3\hbar$ per emitted statistical γ ray [23]. The second consideration deals with the torque exerted by the Coulomb force on each fragment in so far as its symmetry axis is not oriented along the fission axis. This had been already advocated by Strutinsky [24] and Hoffman [7] to account for the totality of the angular momenta of the fragments when rotationally set in motion from rest. The effect of such torques when applied after scission, i.e., on nuclei already set in rotational motion, is evaluated to be small, about or less than $1\hbar$ per fragment [23] (see in particular the estimates of Refs. [25,26]).

These rather long introductory remarks were necessary to put into proper perspective the actual challenge that existing data are presenting to our theoretical approach. Let us draw some conclusions from them. For a certain number of emitted neutrons (close to its average value), because of the various particle emission processes at work and the post-scission interaction, it would be very hazardous to infer from such data the spin of fission fragments at scission with an accuracy better than about $2\hbar$. Our efforts should thus only intend to reproduce orders of magnitude and trends of the fragment spins, for example, as a function of the total excitation (or kinetic) energy or as a function of the fragmentation. Moreover, we must clearly state that we have only discussed above, and will only attempt to describe below, low-energy or even zero-energy (i.e., spontaneous) fission where the total angular momentum in the laboratory system is low (if not exactly vanishing, as in the case of the spontaneous fission of an even-even nucleus). Some preliminary studies of a possible way to release this restriction have been presented in Ref. [27].

III. PREVIOUS THEORETICAL DESCRIPTIONS OF FISSION-FRAGMENT ANGULAR MOMENTA

The most widely considered theoretical explanation of the angular momenta of fission fragments relies on the thermal excitation of collective angular-momentum-carrying modes. Nix and Swiatecki [28] were the first to consider the normal collective modes yielding angular momenta perpendicular to the fission axis (see Ref. [29] for an illuminating discussion of the angular-momentum-bearing modes). The latter specification is consistent with the assumption of axial symmetry. One should then exclude modes that cannot be quantally excited due to the symmetry assumption, namely, the global axial rotation and twisting modes. One is left with the so-called bending and wriggling modes. The first one consists of two opposite rotations of two touching or overlapping spheroidal fragments around an axis perpendicular to the plane formed by their axes of symmetry (here, "opposite" means that one fragment rotates clockwise of an angle θ while the other rotates counter-clockwise by the same angle). In the wriggling mode, the two spheroidal fragments rotate in the same direction around an axis perpendicular to the same plane as defined above, while the global system counter-rotates in such a way as to yield a vanishing total angular momentum, if so desired. A simple quantal Hamiltonian allowing these modes is defined by

$$H = \sum_{i=1}^{2} T_i + V. \tag{1}$$

The first term involves a sum over the rotational kinetic energy T_i of the fragment i, expressed in terms of the corresponding moment of inertia B_i as

$$T_i = -\frac{\hbar^2}{2B_i}\left[\frac{1}{\sin\theta_i}\frac{\partial}{\partial\theta_i}\left(\sin\theta_i\frac{\partial}{\partial\theta_i}\right) + \frac{1}{\sin^2\theta_i}\frac{\partial^2}{\partial{\phi_i}^2}\right], \tag{2}$$

whereas the lowest order approximation of the potential V associated with the restoring forces takes the form

$$V = C_1 \sin^2\theta_1 + C_2 \sin^2\theta_2 - D \sin\theta_1 \sin\theta_2 \cos(\varphi_1 - \varphi_2), \tag{3}$$

with the notations of Ref. [25]. Rasmussen and collaborators [30] were the first to solve the corresponding quantum-mechanical problem, though it was for the special case in which only one of the fragments is deformed. Zielinska-Pfabe and Dietrich [25] yielded solutions in the most general case where both fragments may be deformed; these solutions are still being utilized [26].

The collective-model foundations of such an approach are to be found in what has been developed by and around the Frankfurt group as the so-called nuclear molecule model of Ref. [31], or by Volkov and collaborators (see, e.g., Ref. [32]) within the so-called dinuclear system (DNS) model. While initially developed in the context of heavy-ion collisions, these approaches have been applied to low-energy fission (see, e.g., Refs. [33,34]). The version most generally used to describe fission considers two fragments described by axially symmetrical quadrupole sharp-edged density distributions, which are assumed to always remain approximately attached at two of their poles. This imposes in particular that the vector **R** joining the two centers of mass and the two fragment axes (S_i) of symmetry are coplanar. Since obviously,this touching-pole condition cannot be satisfied exactly for nonvanishing values of the angle between **R** and S_1, the validity of this approach is limited to very small values of this angle (and thus similarly for the angle between **R** and S_2, since the two polar lengths of the fragment density distributions have the same order of magnitude). It clearly implies, in addition, that the center-of-mass distance R (i.e., the norm of **R**) varies with the above-considered angle in a correlated fashion.

As noted in the seminal reference [31], the most complete collective-model description of such a diquadrupole system would involve the consideration of 13 dynamical variables. From them, one should single out one of paramount importance, namely, the internuclear distance, defined by the value of R for instance. In the calculations of Refs. [33,34], as well actually as for the Hamiltonian considered in Eqs. (1)–(3), the variable R is assumed to be approximately or exactly frozen. In its most naive interpretation, this would rely on a hypothetical pocket in the potential-energy surface (PES) of the total system. The existence of such local minima in the fission valleys of the PES is not at all grounded on any available purely microscopic calculations (see, e.g., Refs. [35–37]). The references made, for instance, in Ref. [34] to such pockets found in Refs. [38,39] are of course totally misleading, because they refer in practice to adiabatic fusion valleys which are, in general, irrelevant to the fission process. This academic reference to a molecular equilibrium distance is in practice at variance with the actually used touching-poles approximation, which clearly fixes a distance without connection with the alleged one.

It is probably more physical to assume, in a Born-Oppenheimer fashion, that the relevant degrees of freedom for the spin generation mechanism are fast with respect to the one associated with the "elongation" degree of freedom R, as claimed in Ref. [26]. This imposes, in turn, quite drastic constraints on the collective dynamics. As we will see, our interpretation of this mechanism as an orientation pumping involves, instead, the single-particle motion of nucleons in an instantaneous mean potential which could more easily meet the above adiabaticity criterion. Beyond this approximate or exact freezing of the R variable, the addition of the above-detailed geometrical restrictions dramatically reduces the number of variables to only one.

A detailed discussion of these numerous simplifying assumptions is beyond the scope of this paper. We simply would like to remark that the touching-pole ansatz corresponds in effect to an approximately vanishing tip distance at scission in the language of Ref. [40]. This is contradictory to the outcome of most definitions of the scission points (as, e.g., in Refs. [36,40] or the present paper). Moreover, there is no indication in Ref. [34], for instance, that the values of R yielded in the advocated DNS calculations (of the type in Ref. [38]) are consistent with these vanishing tip distances.

Next, we will briefly discuss the results of previous theoretical approaches.

The pioneering work of Zielinska-Pfabe and Dietrich [25] ignores the dynamics of the R variable as in the above-discussed nuclear molecule and DNS calculations, yet allows the full angular dynamics (dealing with the three relevant angles involved in the problem) and does consider a finite angle-dependent tip distance. The moments of inertia are microscopically calculated through the Inglis-Belyaev cranking formula that includes pairing correlations. The results reproduce the global structure of the fragment angular momenta as a function of the fragment mass, namely, the data from Ref. [41] which exhibit a sawtooth structure (not found, however, in the later data of Ref. [12], as already mentioned). They yield also the correct order of magnitude for these angular momenta upon setting a temperature for the fragments of about 2–3 MeV. This approach, however, meets with at least three difficulties. First of all, to account for the average-spin values, one has to resort to the above-mentioned temperatures which are somewhat too high, at least for reasonable collective phonon energies as given in Ref. [25], assuming the thermalization of the collective degrees of freedom. Second, the Zielinska-Pfabe-Dietrich approach is unable to provide any description of the above-quoted dependence of the angular momenta on the excitation energy [13] defined as the fraction of the fission Q value that does not end up in the total fragment kinetic energy. This is so because this method does not explore the fragment deformation space by constraining on various total kinetic or excitation energies. Finally, this approach is inconsistent with the observed similarities between angular γ-ray distributions of binary and ternary fissions [42], while the latter should clearly perturb the bending mode excitation with respect to what is expected in binary fission.

The work of Ref. [26] presents itself as belonging to the nuclear molecule approach. Actually, it deals with the Hamiltonian of Ref. [25], which includes only the angles between each of the two fragment symmetry axes and **R**. Upon considering the fragment-fragment interaction up to second-order terms in the angles only, they obtain a Hamiltonian of a quantum rotor whose eigensolutions are well known. The fragment angular momenta are trivially deduced from the energies stored in the bending modes $E_i^{(b)}$. In this calculation, the fragment interdistance is frozen to a value that does not come out of a molecular calculation but is linked to the total bending energy $E^{(b)} = E_1^{(b)} + E_2^{(b)}$, thus varying with $E^{(b)}$. Since this energy has some bearing on the excitation energy, the authors of Ref. [26] found out, through some rather crude assumptions on the deformation energies, that in their model the fragment shapes do vary very much with $E^{(b)}$. However, the bending mass parameters are calculated from experimentally deduced moments of inertia of each fragment, thus for yet another set of deformations corresponding to the fragment ground states. For the same reasons as in Ref. [25], this approach cannot attempt to reproduce the observed variation of the angular momenta with the total excitation energy.

The DNS approach of Shneidman *et al.* [34] corresponds, as already discussed, to a single angle dynamics. These authors describe the excitation energy dependence of the fragment angular momenta from a thermal excitation of the considered single bending mode. The specific way, with respect to the pairing correlations treatment, in which the inertia parameter introduced in this Hamiltonian is evaluated is of paramount importance. Indeed, it clearly determines the realistic character, or not, of the resulting bending mode frequency, which in turn yields the angular momentum for a definite excitation energy (or temperature). In that respect, the retained choice of the fragment interdistance is not without consequence, since the frequency is an increasing function of R. This is why the results of this approach could not allow going beyond an approximate reproduction of the trend in the data of Ref. [13]. The agreement that they obtained yields temperatures which are significantly lower than those in Ref. [25], which is consistent with the fact that the bending frequencies of the latter are significantly lower than theirs.

IV. THEORETICAL FRAMEWORK

The above presentation clearly indicates that a realistic modeling of the fission-fragment spins, taking into account in a microscopic way all the relevant collective variables at scission, is still waited for. This is why we do not address the issue of a specific collective description of the nuclear dynamics at scission but rather investigate whether quantum-mechanical arguments could explain *a priori* the bulk of the fission-fragment spins. Our work here will examine microscopically and in closer detail what had been previously proposed and discussed in general terms in Refs. [4,27]. The central result is that in most cases, the bulk of the fission-fragment spins is due to quantal fluctuations rather than to thermal fluctuations. In fact, there is more to angular momentum than a mere rotation of a spatial distribution of matter, as experienced in so-called magnetic rotations [43] or intrinsic vortical modes [44], for instance. Here, we make use of the Heisenberg uncertainty principle as applied to systems whose orientation is somewhat fixed. Since some angular information is known, one gets a quantal distribution of the canonically conjugated variable, hence a finite average angular momentum. It is in that sense that one may say that the orientation "pumps" angular momentum [4].

Let us elaborate briefly on the general meaning of this mechanism. In the quantum mechanics of rotationally invariant systems, it is a well known fact that the spatial distribution of physical states may be viewed (see Ref. [45]) as a weighted average of intrinsic states which may correspond to a deformed distribution of matter. This is no longer the case in spatially polarized systems (e.g., a nucleus embedded in a crystalline site where an electrical quadrupole field is present). There, the physical states are deformed and do correspond to a combination of states which have definite angular momenta. This situation is encountered precisely in our Hartree-Fock-BCS calculations under constraint on the quadrupole moment. When describing, e.g., nuclear equilibrium deformation properties, the resulting wave functions cannot stand as physical approximations of the ground states. For even-even nuclei, for instance, one may think of projecting a 0^+ component out of them. But in polarized systems, on the contrary, the intrinsic states may be arguably thought of as representing physical states. In the present context, near scission, we picture, by mere assumption, the two nascent or just separated fragments as aligned, without dwelling too much here on the mechanism to achieve that, and we claim that our calculated Hartree-Fock-BCS wave functions are reasonable approximations of the fragment wave functions.

The mechanism of orientation pumping may be illustrated in the model case example of a quantum rotor embedded in a polarizing field whose Hamiltonian is written as [46]

$$H = -\frac{\hbar^2}{2\mu}\frac{1}{\sin\theta}\frac{d}{d\theta}\left(\sin\theta\frac{d}{d\theta}\right) + \frac{C}{2}\sin^2\theta, \tag{4}$$

where μ and C denote the inertia and rigidity parameters, respectively. When the polarizing field is strong ($C \gg 1$ in units of $\hbar^2/\mu$), we reach the small angle limit in which H takes the form

$$H \approx -\frac{\hbar^2}{2\mu}\frac{1}{\theta}\frac{d}{d\theta}\left(\theta\frac{d}{d\theta}\right) + \frac{C}{2}\theta^2. \tag{5}$$

As derived in Appendix A, the corresponding ground-state wave function Ψ_0 is exactly given by

$$\Psi_0(\theta) = N_0\, e^{-\frac{\theta^2}{2\theta_0^2}}. \tag{6}$$

where θ_0 is written, in terms of the inertia and rigidity parameters, as

$$\theta_0 = \sqrt{\hbar}(\mu C)^{-1/4}, \tag{7}$$

and N_0 is a normalization factor. Since $C \gg 1$, we have $\theta_0 \ll 1$. We may then expand $\Psi_0(\theta)$ onto good angular-momentum wave functions $Y_\ell^0(\theta)$ (spherical harmonics) taking into account the axial symmetry of Ψ_0 as

$$\Psi_0(\theta) = \sum_{\ell=0}^{\infty} a_\ell Y_\ell^0(\theta). \tag{8}$$

It is found (see Appendix A) that the expansion coefficients a_ℓ take the form, in the limit $\theta_0 \ll 1$,

$$a_\ell \approx \theta_0 \sqrt{2\ell + 1}\, e^{-\frac{\theta_0^2}{2}\ell(\ell+1)}. \tag{9}$$

This yields a finite expectation value of the square of the angular-momentum operator $\hat{\mathbf{L}}^2$

$$\langle \Psi_0 | \hat{\mathbf{L}}^2 | \Psi_0 \rangle \approx \frac{1}{\theta_0^2}, \tag{10}$$

hence the large average value $\bar{\ell} \approx 1/\theta_0$. This is an example of angular-momentum pumping for such a system constrained to move in a restricted angular domain. Note that our one-dimensional orientation-pumping model Hamiltonian (5) is a special case of a quantum rotor for which we consider the lowest mode having $m = 0$ (see Appendix A).

Let us come back now to our fission context. We assume that the wave function Φ of a scission configuration, defined in the next section, is reasonably well described as a product of two separated wave functions, typically as two BCS wave functions Φ_i $(i = 1, 2)$. To obtain the angular-momentum value arising from the orientation pumping alone, we discard any other source of fragment angular momentum. We therefore consider the case of spontaneous fission of an even-even nucleus in two fragments whose relative orbital momentum is vanishing. The relative motion of the two fragments is thus in an s state, noted Φ_{rel}. Since the most probable fragments formed in the fission of actinides have axially symmetric shapes in their ground states, the whole system—hence each fragment—is assumed to possess axial symmetry with the symmetry axis aligned in the fission direction. Upon projecting Φ_i on good angular-momentum (I, M) states denoted by $\Psi_i(I, M)$, with expansion coefficients $a_I^{(i)}$,

$$\Phi_i(M_i) = \sum_I a_I^{(i)} \Psi_i(I, M_i), \tag{11}$$

and coupling them to a total zero angular momentum (conserved throughout the spontaneous-fission process), we obtain [4]

$$\begin{aligned} \Phi \;=\; & \delta_{M_1,-M_2} \Phi_{\text{rel}} \sum_{I,M} \frac{(-1)^{M_1+M}}{2I+1} a_I^{(1)} a_I^{(2)} \\ & \times \Psi_1(I, M) \Psi_2(I, -M). \end{aligned} \tag{12}$$

The expectation value $\langle \hat{\mathbf{J}}_i^2 \rangle$ of the square of the angular momentum operator of each fragment $\hat{\mathbf{J}}_i^2$ in the global state Φ is then given by

$$\left\langle \hat{\mathbf{J}}_i^2 \right\rangle = \frac{\langle \Phi | \hat{\mathbf{J}}_i^2 | \Phi \rangle}{\langle \Phi | \Phi \rangle} = \langle J^2 \rangle, \tag{13}$$

where

$$\langle J^2 \rangle = \frac{\sum_I \frac{I(I+1)}{2I+1} \left| a_I^{(1)} \right|^2 \left| a_I^{(1)} \right|^2}{\sum_I \frac{1}{2I+1} \left| a_I^{(1)} \right|^2 \left| a_I^{(1)} \right|^2}. \tag{14}$$

As expected for angular-momentum conservation reasons, $\langle \hat{\mathbf{J}}_i^2 \rangle$ is independent of i. This is an exact orientation-pumping result for the fission-fragment spins. In passing, it may be noted that contrary to an erroneous statement in Ref. [34], the treatment of Ref. [4] deals with states that are clearly eigenstates of the angular momentum, since they result from the explicit application of a projector on a global zero-spin state [see Eq. (1) of Ref. [4]]. Nevertheless, a caveat should be made here. When we refer to "exact" calculations, we mean as far as the treatment of the various angular-momentum components of the fragment wave functions are concerned. However, in the case of strong shape fluctuations (such as soft vibrations around some minimum, in particular, of a spherical shape), this treatment would clearly break down.

With the restriction to the case of no shape fluctuations, going any further with such a general formalism would require us to perform the above-mentioned projection calculations, which is beyond the scope of the present work. Therefore, we resort to using an approximation for the expansion coefficients $a_I^{(i)}$. More precisely, we assume that both fragments are rigidly deformed and approximate $a_I^{(i)}$ by the expression given in Eq. (9) for a strongly constrained quantum rotor. In doing so, we interpret from Eq. (10) the θ_0^2 parameter as the inverse of the intrinsic expectation value $\langle J_i^2 \rangle_{\text{intr}}$ of the $\hat{\mathbf{J}}_i^2$ operator evaluated for the wave function Φ_i of the fragment i. Therefore, we have

$$\left| a_I^{(i)} \right|^2 = \frac{2(2I+1)}{\left\langle J_i^2 \right\rangle_{\text{intr}}} \exp\left(-\frac{I(I+1)}{\left\langle J_i^2 \right\rangle_{\text{intr}}} \right). \tag{15}$$

Finally, in the large quantum number limit reached when $\langle J_i^2 \rangle_{\text{intr}} \gg 1$, Eq. (14) becomes

$$\langle J^2 \rangle = \left(\frac{1}{\left\langle J_1^2 \right\rangle_{\text{intr}}} + \frac{1}{\left\langle J_2^2 \right\rangle_{\text{intr}}} \right)^{-1}. \tag{16}$$

As a result, if one fragment is spherical, then Eq. (16) yields vanishing fragment spins. However, we clearly reach then the limits of application of the so-called exact orientation-pumping description.

To conclude this section, let us clearly point out the various levels of assumptions that may be considered in an orientation-pumping theoretical framework.

First, we assume that the system at scission may be represented by a wave function, in other words that we still deal with a pure case (no temperature). Then we proceed by prescribing the separability of the total wave function in three parts $|\Phi\rangle = |\Phi_1\rangle \otimes |\Phi_2\rangle \otimes |\Phi_{\text{rel}}\rangle$, where $|\Phi_i\rangle$ denotes the wave function of the fragment i and $|\Phi_{\text{rel}}\rangle$ describes the relative motion.

Then we may further assume that there is no relative angular momentum and that the fragment wave functions may be approximated by BCS vacuum wave functions. This excludes at this stage any shape fluctuations (vibrations, configuration mixing, etc.), the description of quasiparticle excitations, hence most of the isomers which are seen in actual fission, and the effects resulting from nonvanishing relative angular motion. From angular-momentum conservation arguments, the two latter points are in fact connected.

The last level of approximation is actually the one at which we stand in this paper. We perform an approximate projection assuming a pure-rotor character of the projected energies together with less restrictive side assumptions. Without specific modifications, this clearly excludes any possibility of providing a fair description of fragments that are spherical in their ground states.

Consequently, in the limits of this paper, we can only treat even-even fragmentations where the fragments are somewhat rigidly deformed and not in quasiparticle isomeric states. Of course, to compare our results with existing data, we will have to compromise the rigid-deformation condition to deal here with fragmentation in the ^{252}Cf spontaneous fission for which experimental data are available. Any failure in a fair description of the data could not be necessarily attributed to the orientation pumping itself, which after all follows from basic laws of quantum mechanics for spatially polarized objects, but to any of the above-listed approximations.

V. SCISSION CONFIGURATIONS

Whatever model is used to evaluate the fission-fragment angular momenta, one has to define the scission configuration. This is the subject of this section.

A. Definition of scission

In the course of a fission process, we may single out the particular time at which the nuclear density in the neck region between the nascent fragments may be considered as vanishing. In an independent-particle approximation or for a correlated system considering the canonical basis states (diagonalizing the one-body density matrix $\hat{\rho}$), after such a time we would ideally expect that the wave function of any nucleon spreads over only one fragment. Therefore, after this event of separation, a given nucleon should then belong to only one fragment, and the dynamics of nucleons in one of the fragments $\mathcal{F}_1$ become independent of their nuclear interactions with nucleons in the other fragment $\mathcal{F}_2$. The dynamics of nucleons in $\mathcal{F}_1$ would be therefore governed only by the internal interactions and the external Coulomb potential created by $\mathcal{F}_2$ and decreasing with time. This particular point in the fission process is called the scission point.

In practice, however, in Hartree-Fock, Hartree-Fock-BCS, or Hartree-Fock-Bogoliubov (HFB) calculations, the individual wave functions are well defined, but there is of course no guarantee that they will belong totally to either fragment, whose particle numbers, moreover, are merely defined by constraining the relevant expectation values. Nevertheless, the one-body density function $\rho(\mathbf{r})$, i.e., the diagonal matrix element in $\mathbf{r}$ of $\hat{\rho}$, is well defined as a whole, and its separation into two pieces corresponding to the fission fragments may be judged from purely geometrical arguments. This is actually one of the criteria that Goutte and collaborators retained to define scission in their HFB calculations [36].

Instead, we choose to rely on a dynamical criterion. Assuming that we are able to define nascent or separated fragments, we should try to analyze the forces acting between the two fragments. To this end, in a fashion suited to the quantal character of the problem, we must consider an average over the many nucleon-nucleon interactions. Within an approximate many-body treatment, we may evaluate the potential-energy surface from an effective nucleon-nucleon interaction for a relevant set of collective dynamical variables. In a simple version of that program, we may rather use a phenomenological interaction potential, such as the Yukawa-plus-exponential (YPE) potential proposed by Krappe, Nix, and Sierk [47]. From the knowledge of this potential energy, we might derive forces upon taking their derivatives with respect to a collective deformation variable that varies in time much slower than the other variables. A natural scission criterion would then be expressed in terms of the ratio of the resulting nuclear $\mathbf{F}_N$ and Coulomb $\mathbf{F}_C$ forces as

$$\frac{|\mathbf{F}_N|}{|\mathbf{F}_C|} = \eta, \tag{17}$$

where $|\mathbf{F}|$ denotes the norm of the vector $\mathbf{F}$ and η takes a small value considered as a free parameter. However, a clear separation of the time scales involved in the motion is far from being guaranteed *a priori*. In view of this and to handle a simple determination of the scission point, we replace the forces in the above ratio with the corresponding nuclear E_N and Coulomb E_C interaction energies:

$$\left|\frac{E_N}{E_C}\right| = \eta. \tag{18}$$

With this prescription, the scission point occurs whenever the above ratio becomes lower than a critical value of the constant η. Here η should be regarded as a model parameter of which the lack of prediction reflects the elusive character of the scission concept.

B. Semimicroscopic description of scission configurations

We now come to the description of the configurations of a fissioning nucleus at scission. Since we are interested in spontaneous fission, the initial state of this nucleus is its ground state, with energy E_{GS}. Assuming that this nucleus is an isolated system undergoing fission by tunneling, its total energy E_{tot} is conserved.

After tunneling through the fission barrier, the nucleus appears at points called here exit points exhibiting configurations with a highly pronounced neck. We consider that a fissioning nucleus can only reach scission configurations that lie beyond (with respect to a global elongation variable) the exit points and, of course, whose energies are less than or equal to the ground-state energy. To the scission criterion given by Eq. (18), we therefore have to add the following condition:

$$E_{\mathrm{sc}} \leqslant E_{\mathrm{GS}}, \tag{19}$$

where E_{sc} denotes the scission-configuration energy. The scission configurations obeying the relations (18) and (19) correspond to well-separated fragments. We are thus able to decompose the energy of the whole system at scission as

$$E_{\text{sc}} = E_C + E_N + \sum_{i=1}^{2} E_i^{(\text{sc})}. \tag{20}$$

In the last term of Eq. (20), $E_i^{(\text{sc})}$ represents the self-energy of the nucleons belonging to the partner i of the scission configuration.

In all microscopic studies of potential-energy surfaces, the potential part of Hamiltonian $\hat{H}$ of the fissioning nucleus is taken as an effective phenomenological two-body interaction (usually of Skyrme or Gogny type). Although the expectation value of $\hat{H}$ can in principle be calculated at any point of the energy surface, it is difficult to extract the four contributions of the right-hand side of Eq. (20) because this requires one to disentangle the self-energies $E_i^{(\text{sc})}$ and the interaction energies E_N and E_C. This is quite difficult and partly ambiguous *a priori* because the Hamiltonian, as a whole, is a nonlocal operator. Furthermore, to compute the fragment self-energies, one has to unfold the local densities entering the energy-density functional into sums of two sets of densities localized each fragment (with some overlap in the neck). This has been done in the case of two spherical nuclei with the Skyrme interaction by Pomorski and Dietrich [48], who showed that the resulting interaction potential is similar to the YPE potential. For that reason and because we do not expect that the conclusions drawn from the final results should significantly depend on the refinement in the calculation of E_N, we have decided in the present exploratory study to follow a semimicroscopic approach.

We describe a scission configuration as two axially symmetric fragments with a common symmetry axis and neglect the mutual Coulomb polarization effect on each fragment. Since the ground-state shapes of the considered nuclei (in the mass region $A \approx 110$ to $A \approx 140$) do not exhibit any energetically significant octupole distortions [49], we further assume left-right reflection symmetry for each of them. In this context, a scission configuration may thus be reasonably well characterized by three shape degrees of freedom: the center-of-mass distance $D_{\text{c.m.}}$ and the elongation of each fragment, expressed as the axial quadrupole moment $Q_{20}^{(i)}$ given by

$$Q_{20}^{(i)} = \int_{\mathcal{F}_i} d^3\mathbf{r}\,\rho(\mathbf{r})(2z^2 - x^2 - y^2). \tag{21}$$

In the above expression $\rho(\mathbf{r})$ denotes the total nuclear density (neutron and proton contributions), and the integration is performed over the nuclear volume of fragment $\mathcal{F}_i$. The fragment energy E_i is therefore assumed to depend only on $Q_{20}^{(i)}$ and is calculated separately for each fragment in the Skyrme-Hartree-Fock-BCS approach previously applied to studies involving very large deformations [50–52]. As for the nuclear interaction energy between the two fragments, it has been approximated by its value taken for equivalent coaxial spheroids using the YPE potential (with the parameters of Ref. [53]). By "equivalent spheroids" we mean those having the same elongation $Q_{20}^{(i)}$ and root-mean-square radii $R_{\text{r.m.s}}^{(i)}$ as the actual fragments. Similarly, the Coulomb interaction energy has been calculated for the equivalent spheroids using the exact analytical expression of Ref. [54] (see Appendix B). Given the scission conditions (18) and (19), the center-of-mass distance can be considered as a function of $Q_{20}^{(1)}$ and $Q_{20}^{(2)}$. The space of scission configurations is therefore two-dimensional and restricted to certain regions, because the condition expressed in Eq. (19) limits the variations of $Q_{20}^{(1)}$ and $Q_{20}^{(2)}$.

Finally, it is worth mentioning that the above modeling of scission configurations is formally similar to the one sketched in Ref. [55]. An important difference, however, lies in the way $D_{\text{c.m.}}$ is treated (or equivalently, the tip distance d). In the present model, the condition in Eq. (18) leads to a distribution of $D_{\text{c.m.}}$ values, hence a distribution of tip distances, whereas the work of Ref. [55] considered a fixed d value.

VI. PUMPING OF FISSION-FRAGMENT ANGULAR MOMENTUM AS A FUNCTION OF FRAGMENT TOTAL EXCITATION ENERGY

In the above-described orientation-pumping mechanism, both fragments have the same spin J_f defined by

$$J_f(J_f + 1) = \langle J^2 \rangle, \tag{22}$$

where $\langle J^2 \rangle$ is calculated within the approximation of Eq. (16). As mentioned in the previous section, we neglect the polarization effect on each fragment, so we use the BCS wave function of the isolated nucleus i to compute the expectation value of the $\hat{\mathbf{J}}^2$ operator and obtain $\langle J^2 \rangle_{\text{intr}}^{(i)}$ as a function of $Q_{20}^{(i)}$.

To calculate J_f as a function of the fragment total excitation energy (TXE), we need to establish the expression of TXE in terms of known quantities. For this purpose, we recall that we deal here with the spontaneous fission of an isolated nucleus initially in its ground state. We can express its conserved energy E_{tot} at three different stages of the fission process:

(i) In the initial state, the fissioning nucleus energy is simply

$$E_{\text{tot}} = E_{\text{GS}}. \tag{23}$$

(ii) At scission, we have

$$E_{\text{tot}} = E_{\text{sc}} + E_{\text{free}}, \tag{24}$$

which defines the available energy at scission, called "free energy" in Ref. [40] and noted here E_{free}

(iii) At the end of the acceleration phase of the primary fragments (assuming thus no prescission or near-scission neutron emission), E_{tot} takes the form

$$E_{\text{tot}} = Q + \sum_{i=1}^{2} E_i^{(\text{GS})}, \tag{25}$$

where Q is the energy released by the fission reaction and $E_i^{(\text{GS})}$ the ground-state energy of the fragment i.

Defining the fragment deformation energy $E_{\rm def}^{(i)}$ at scission with respect to its ground-state value by

$$E_{\rm def}^{(i)} = E_i^{(\rm sc)} - E_i^{(\rm GS)} \tag{26}$$

and using the fact that the nuclear interaction energy E_N is negligible according to the scission criterion of Eq. (18), we can write the energy released by the fission reaction in the following two different ways:

$$Q = E_C + E_{\rm free} + \sum_{i=1}^{2} E_{\rm def}^{(i)} \tag{27}$$

or

$$Q = {\rm TKE} + {\rm TXE}, \tag{28}$$

where TKE denotes the total kinetic energy of the fission fragments.

The available energy at scission $E_{\rm free}$ is assumed to be shared between a collective kinetic component $E_{\rm K}$ and an intrinsic excitation component $E_{\rm intr}$. The kinetic contribution is the so-called prescission kinetic energy acquired by the fragments during their descent from saddle to scission. The intrinsic excitation contribution is an energy shared among the noncollective degrees of freedom. It results from the dissipation of part of the gain of potential energy ($E_{\rm free}$) during the descent from saddle to scission. We can thus write

$$E_{\rm free} = E_{\rm K} + E_{\rm intr}. \tag{29}$$

From Eqs. (27) and (28), it is clear that the expressions of TKE and TXE in terms of E_C, $E_{\rm def}^{(i)}$, and $E_{\rm free}$ are not uniquely determined. The physical reason for this is the existence of a distribution for TKE and TXE even when Q is fixed. Here, we assume that the Coulomb interaction energy is totally converted into kinetic energy and that the fragment deformation energies contribute only to TXE. As for the two components of $E_{\rm free}$, they are shared according to their definition; hence we obtain the following expressions for TKE and TXE:

$$\text{TKE} = E_C + E_{\rm K}, \tag{30}$$

$$\text{TXE} = \sum_{i=1}^{2} E_{\rm def}^{(i)} + E_{\rm intr}. \tag{31}$$

To describe the splitting of $E_{\rm free}$ according to Eq. (29), we introduce a parameter f defined by $E_{\rm K} = fE_{\rm free}$, so the expressions of TKE and TXE finally read

$$\text{TKE} = E_C + fE_{\rm free}, \tag{32}$$

$$\text{TXE} = \sum_{i=1}^{2} E_{\rm def}^{(i)} + (1-f)E_{\rm free}. \tag{33}$$

Out of the three-dimensional (3D) collective space ($D_{\rm c.m.}$, $Q_{20}^{(1)}$, $Q_{20}^{(2)}$), upon defining the scission configurations associated with a given TXE value by Eqs. (18) and (33), we define a subspace of dimension 1 comprised of an infinite number of such configurations. In general, this subspace forms in the 3D space a skew curve (as opposed to a plane curve) $\mathcal{C}_{\rm TXE}$, which can be parametrized by a curvilinear abscissa s as explained in Appendix C. However, as will be discussed in Sec. VII B, the surface representing the function $D_{\rm c.m.}(Q_{20}^{(1)}, Q_{20}^{(2)})$ appears to be single valued, very smooth, and as a matter of fact rather well approximated by a plane in the region of interest. This is why we will represent, in the following, the curve $\mathcal{C}_{\rm TXE}$ by its projection on the ($Q_{20}^{(1)}$, $Q_{20}^{(2)}$) plane and, accordingly, discuss the variations of TXE at scission as a function of $Q_{20}^{(1)}$ and $Q_{20}^{(2)}$.

To define specifically the curvilinear abscissa s, we need to redefine our choice of collective variables so as to ensure their consistency (same units, comparable range of variations). More importantly, we need to choose a metric in the resulting 3D space. Without undertaking definite mechanical studies implying the relevant potential energy and inertia parameters, it is impossible to avoid making rather arbitrary choices for both the definition of the collective variables and the associated metric. The three collective variables which we consider are the three components of the total quadrupole moment $Q_{20}^{(\rm tot)}$, namely, $Q_{20}^{(1)}$, $Q_{20}^{(2)}$, and Q_D, where the latter is defined by

$$Q_D = Q_{20}^{(\rm tot)} - Q_{20}^{(1)} - Q_{20}^{(2)} = \frac{2A_1A_2}{A_1+A_2} D_{\rm c.m.}^2. \tag{34}$$

In Eq. (34), A_i denotes the nucleon number of fragment i. As for the metric, we find it appropriate not to single out one dynamical variable over the others and thus adopt the Cartesian metric

$$ds^2 = \left(dQ_{20}^{(1)}\right)^2 + \left(dQ_{20}^{(2)}\right)^2 + (dQ_D)^2. \tag{35}$$

The practical issues related to the calculation of the curvilinear abscissa s are detailed in Appendix C.

The distribution over the scission configurations should result from a relevant quantal calculation for the collective dynamics. To mock it up in this exploratory study, we assume a weight of the form

$$w = e^{-E_{\rm sc}/\Theta}. \tag{36}$$

It is important to note that even though the simulation of the spreading among scission configurations seems to refer to the approach of Wilkins and collaborators [56], it is different in spirit, because we have invoked here not a thermal distribution but rather a purely quantal fluctuation. The latter yields a Gaussian distribution in the curvilinear abscissa s when, at a given TXE, $E_{\rm sc}$ varies quadratically with s around its minimum. However, this clearly holds only when the collective-energy parameter Θ is smaller than or comparable to the maximum energy range (over its local equilibrium value) in which a harmonic approximation is substantiated. In the physical situations discussed below, this will not be always the case as discussed in the next sections together with an assessment of a suitable range for the numerical values of Θ.

The above-defined probability distribution enables us to average J_f over the solutions of Eqs. (18), (24), and (33) for a fixed TXE value by a curvilinear integration on the contour $\mathcal{C}_{\rm TXE}$

$$\overline{J_f} = \frac{1}{\mathcal{N}} \int_{\mathcal{C}_{\rm TXE}} ds\, J_f\left(Q_{20}^{(1)}(s), Q_{20}^{(2)}(s)\right) w(s), \tag{37}$$

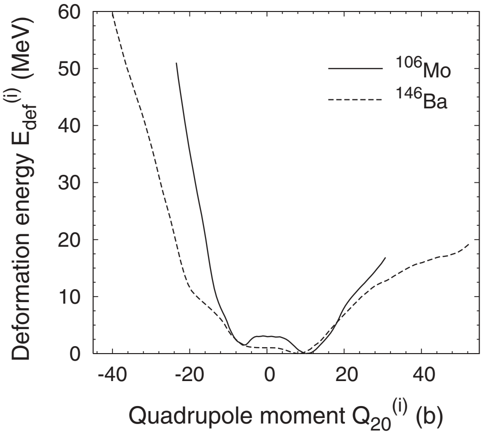

FIG. 1. Potential energy of deformation $E_{\mathrm{def}}^{(i)}$ of ^{106}Mo and ^{146}Ba with respect to their respective ground-state values as a function of the axial quadrupole moment $Q_{20}^{(i)}$.

with the normalization factor $\mathcal{N}$

$$\mathcal{N} = \int_{\mathcal{C}_{\mathrm{TXE}}} ds\, w(s). \tag{38}$$

In practice, as discussed in Appendix C, we discretized the $(Q_{20}^{(1)}, Q_{20}^{(2)})$ space and checked that the final results are not significantly sensitive to the mesh size.

VII. RESULTS AND DISCUSSION

As mentioned earlier, the main objective of this study is to calculate the average fragment spin $\overline{J_f}$ as a function of the fragment total excitation energy TXE. In the process of constructing this curve, we start with a presentation of the different ingredients that contribute to it, so as to help understand the final result.

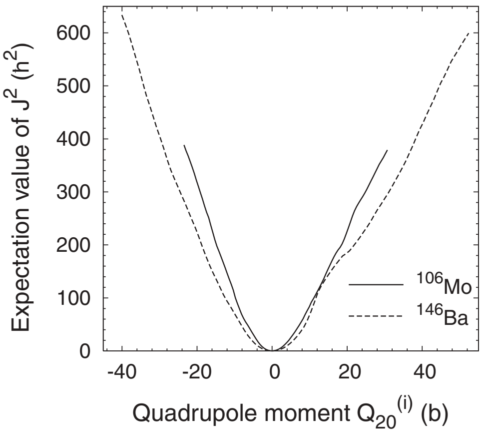

FIG. 2. Expectation value of $\hat{\mathbf{J}}^2$ (in $\hbar^2$) as a function of the quadrupole moment for ^{106}Mo and ^{146}Ba.

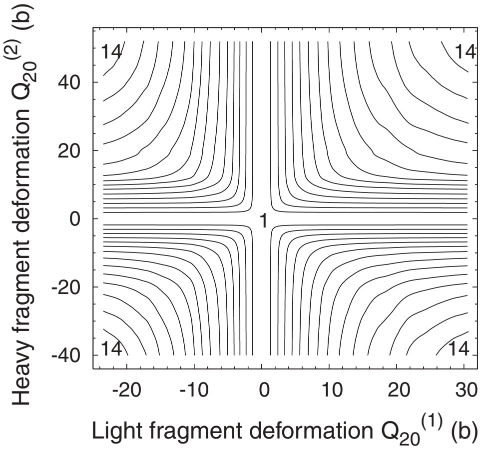

FIG. 3. Contour map of J_f (in $\hbar$) as a function of fragment elongation for the fragmentation ^{106}Mo+^{146}Ba. Contours range from 1 (innermost contours labeled "1") to 14 (outermost contours labeled "14"), with a $1\hbar$ step.

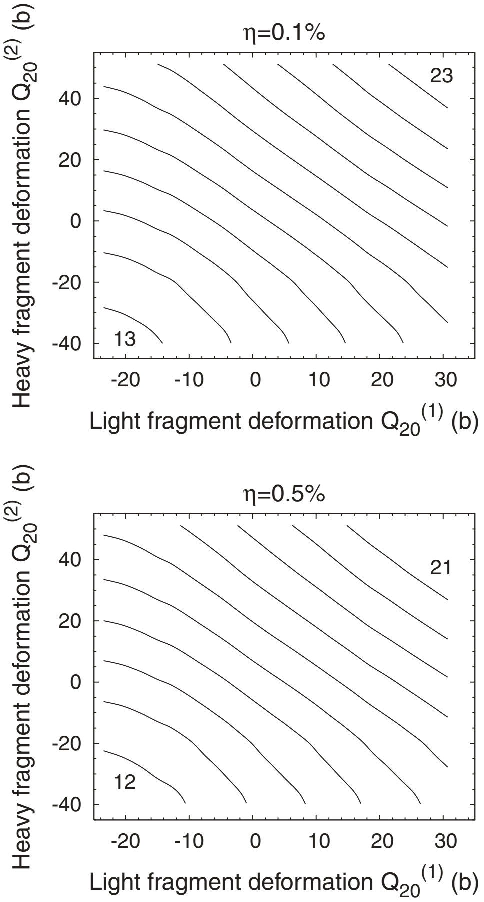

FIG. 4. Contour maps of $D_{\mathrm{c.m.}}$ at scission. The first contour in the bottom left corner corresponds to $D_{\mathrm{c.m.}} = 13$ fm for the upper panel ($\eta = 0.1\%$) and to $D_{\mathrm{c.m.}} = 12$ fm for the lower one ($\eta = 0.5\%$). As one increases the fragment deformations the $D_{\mathrm{c.m.}}$-values increases by 1 fm.

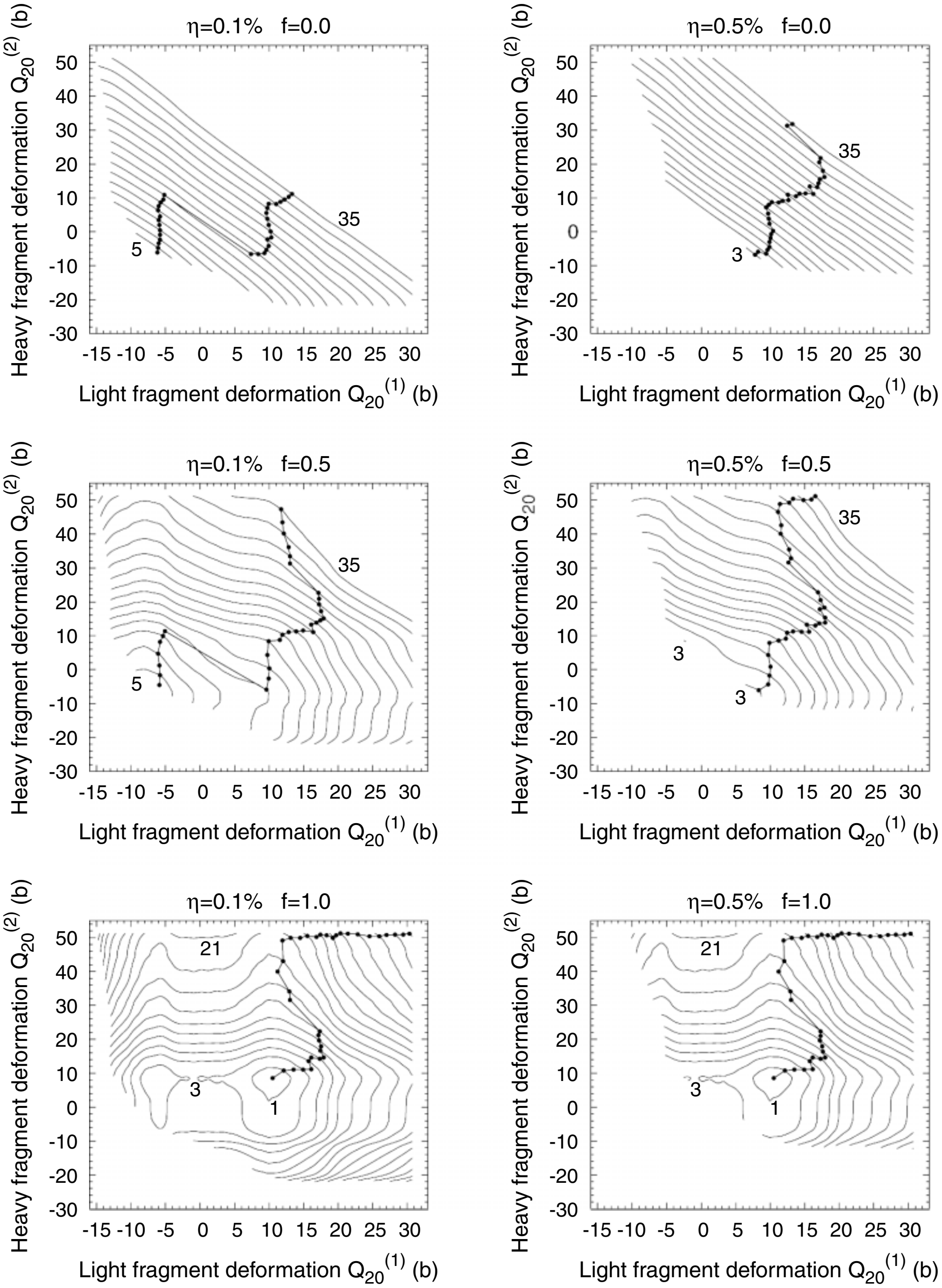

FIG. 5. Contour maps of TXE at scission from 0 to 35 MeV for ^{106}Mo+^{146}Ba scission configurations obtained with the YPE nuclear potential for two different η values and three different values of f. Dots indicate the location on each level contour of the scission configuration having the lowest value of the potential energy $E_{\rm sc}$ defined by Eq. (20).

A. Hartree-Fock calculations of fragment properties

As already discussed, we retain here the ^{106}Mo+^{146}Ba fragmentation. In the following, the index or superscript $i = 1$ denotes the light fragment (^{106}Mo), whereas $i = 2$ corresponds to the heavy fragment (^{146}Ba). We start by computing the deformation energy curves for both fragments within the constrained Hartree-Fock-BCS approach. As in Ref. [50], we use the Skyrme SkM* effective interaction in the mean-field channel and the seniority force in the pairing channel. The strength of the seniority force has been adjusted for neutrons and protons so as to reproduce the experimental odd-even mass differences (see, e.g., Ref. [57] for a discussion of such a determination). In view of the arguments of Ref. [58], a three-point formula is used for each charge state q and each fragment i. The pairing matrix elements $V_q^{(i)}$ are given in terms of the constants $G_q^{(i)}$ entering the description of pairing correlations by

$$V_q^{(i)} = \frac{G_q^{(i)}}{11 + N_q^{(i)}}, \tag{39}$$

where $N_q^{(i)}$ denotes the number of particles of type q in the fragment i. The corresponding values of $G_q^{(i)}$ obtained here for ^{106}Mo and ^{146}Ba are given in Table I for an active pairing window comprised of all levels up to 6 MeV above the chemical potential. In addition, according to the method and notations of Ref. [59], a smooth cutoff with a diffuseness parameter $\mu = 0.2$ MeV was used.

TABLE I. Neutron (G_n) and proton (G_p) pairing strengths of ^{106}Mo and ^{146}Ba used in Eq. (39) to calculate the pairing matrix elements and adjusted to the experimental odd-even mass difference from a three-point formula.

Nucleus	G_n (MeV)	G_p (MeV)
^{106}Mo	16.2	15.6
^{146}Ba	14.3	16.2

We expand our single-particle states in a cylindrical harmonic-oscillator basis that includes 17 major shells. This basis size is large enough to ensure that the deformation energy depends weakly on the basis parameters b and q (with the notation of Ref. [60]). An approximate optimization of b and q, according to the method proposed in Ref. [60], is therefore appropriate, all the more so because the nuclear shapes depart moderately from spheroids in the deformation range considered here. The obtained potential energy of deformation, calculated with respect to the ground-state value (corresponding to the lowest minimum) and upon assuming axially symmetric shapes, is represented in Fig. 1 for ^{106}Mo and ^{146}Ba as a function of the axial quadrupole moment Q_{20}.

The deformation-energy curves of the two nuclei exhibit different patterns. The lighter nucleus has two local minima at finite deformations, one oblate and one prolate, the latter being the lowest. The ground-state deformation of ^{106}Mo is therefore prolate, with $Q_{20} \approx 10$ b. In contrast, the deformation-energy curve of ^{146}Ba merely exhibits a shallow, prolate minimum. Consequently, we may conclude that the retained fragmentation does not fully meet the rigidly deformed requirement which would allow us to apply Eq. (16) near the fragment equilibrium deformations. As stated already, we have to compromise the validity range of our present simple formula Eq. (16) with the existence of relevant data.

For each deformation point actually calculated along the deformation-energy curves, we also calculate the expectation value of the $\hat{\mathbf{J}}^2$ operator in the associated BCS state $|\Psi_i\rangle$

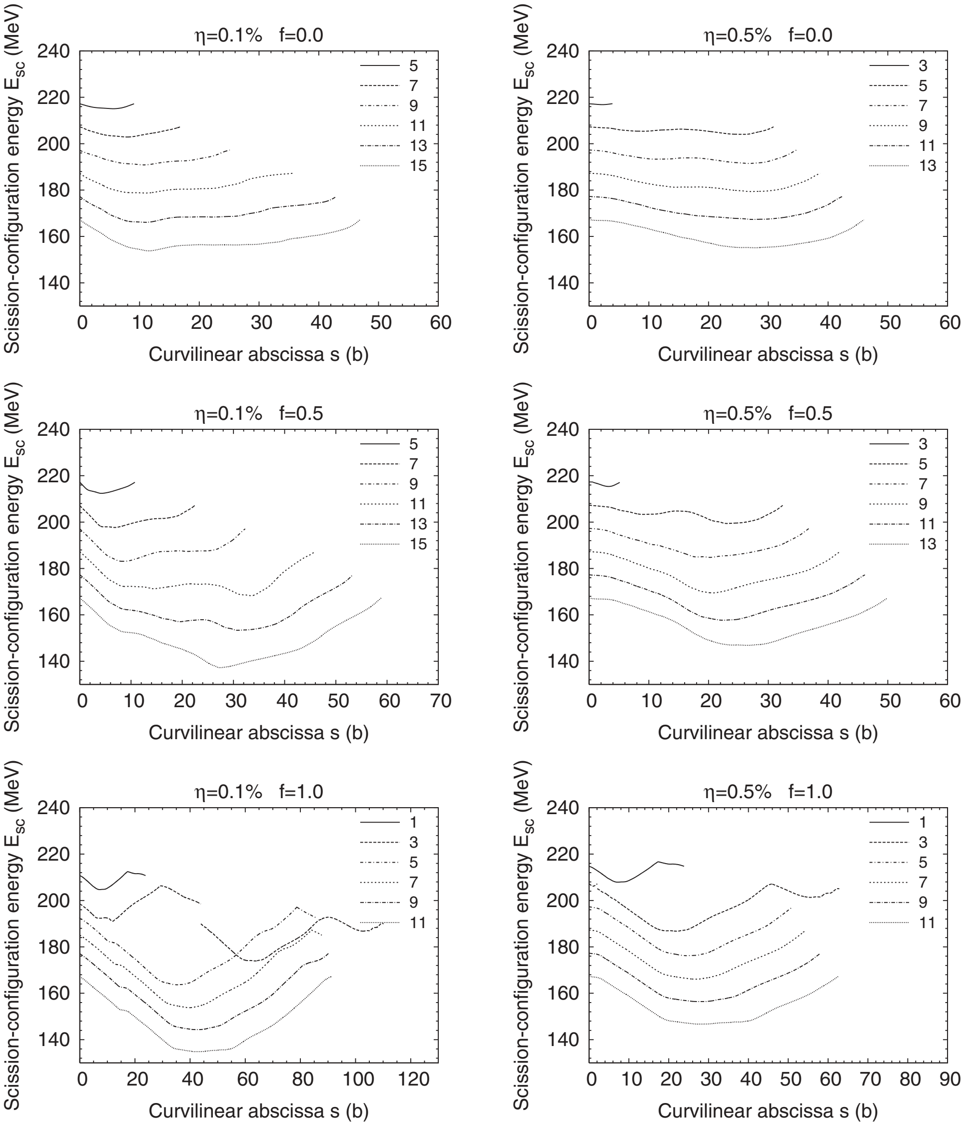

FIG. 6. Variation of the scission-configuration energy E_{sc} along the various TXE contours (whose values are indicated in MeV in the legend) for the six combinations of η and f values.

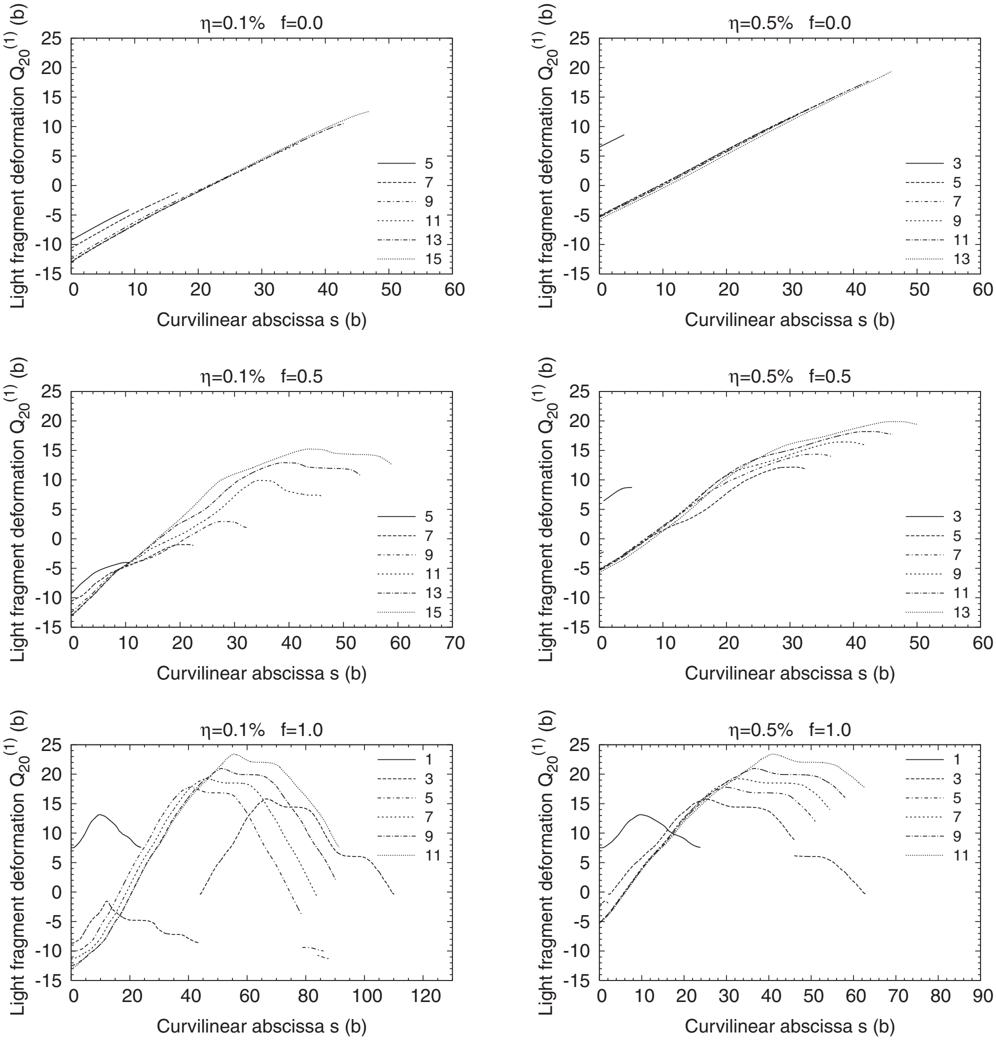

FIG. 7. Same as Fig. 6, but for the quadrupole moment of the light fragment $Q_{20}^{(1)}$.

(normalized to unity) as in Ref. [61], that is,

$$\begin{aligned}\langle J^2\rangle_{\rm intr}^{(i)} &= \langle\Psi_i|\hat{\mathbf{J}}^2|\Psi_i\rangle\\ &= 2\sum_k{}' \langle k|\hat{\mathbf{j}}^2 - \hat{j}_z^2|k\rangle v_k^2\\ &\quad -2\sum_{k,l}{}' |\langle k\hat{j}_+|l\rangle|^2\big(v_k^2v_l^2 + u_kv_ku_lv_l\big)\\ &\quad -\sum_{k,l}{}'' |\langle k|\hat{j}_+|\bar{l}\rangle|^2\big(v_k^2v_l^2 + u_kv_ku_lv_l\big), \qquad (40)\end{aligned}$$

where $|k\rangle$, $|l\rangle$ are single-particle states, $|\bar{k}\rangle$, $|\bar{l}\rangle$ are their time-reversed respective partners, and v_k, u_k the associated BCS factors with the usual notations. The sums $\sum'$ in Eq. (40) run over the single-particle states having a positive eigenvalue Ω of $\hat{j}_z$, whereas the sum $\sum''$ involves only the states having $\Omega = 1/2$. The variation of $\langle J^2\rangle_{\rm intr}$ with Q_{20} is shown in Fig. 2 for both fragments.

As expected, $\langle J^2\rangle_{\rm intr}$ increases as the fragments deform. Note that it varies almost quadratically with $|Q_{20}^{(i)}|$ around 0.

B. Variation of scission properties along TXE contours

For a given scission configuration, the fission-fragment spin J_f is computed from Eqs. (22) and (16). It is therefore a function of the fragment deformations $Q_{20}^{(1)}$ and $Q_{20}^{(2)}$. The level contours of J_f in the $(Q_{20}^{(1)}, Q_{20}^{(2)})$ plane are displayed in Fig. 3.

As expected, J_f vanishes along the $Q_{20}^{(1)}$ and $Q_{20}^{(2)}$ axes. Indeed, when at least one nucleus is spherical, the corresponding intrinsic expectation value $\langle J^2\rangle_{\rm intr}$ vanishes and so does $\langle J^2\rangle$ from Eq. (16), hence $J_f = 0$ from Eq. (22). Moreover, the approximate quadratic variation of $\langle J^2\rangle_{\rm intr}$ with $Q_{20}^{(i)}$ noted earlier explains the $1/(Q_{20}^{(1)})^2$ behavior of the level contours observed in Fig. 3, especially close to the origin.

As discussed in Sec. VI, the calculation of $\overline{J_f}$ as a function of TXE requires one to average J_f over an infinite number of scission configurations with the probability distribution w given by Eq. (36). In the rest of this subsection, we present the variation of relevant fragment properties along the TXE contours $\mathcal{C}_{\rm TXE}$.

In principle, we should consider these contours in the 3D space spanned by $Q_{20}^{(1)}$, $Q_{20}^{(2)}$, and $D_{\rm c.m.}$. However, a

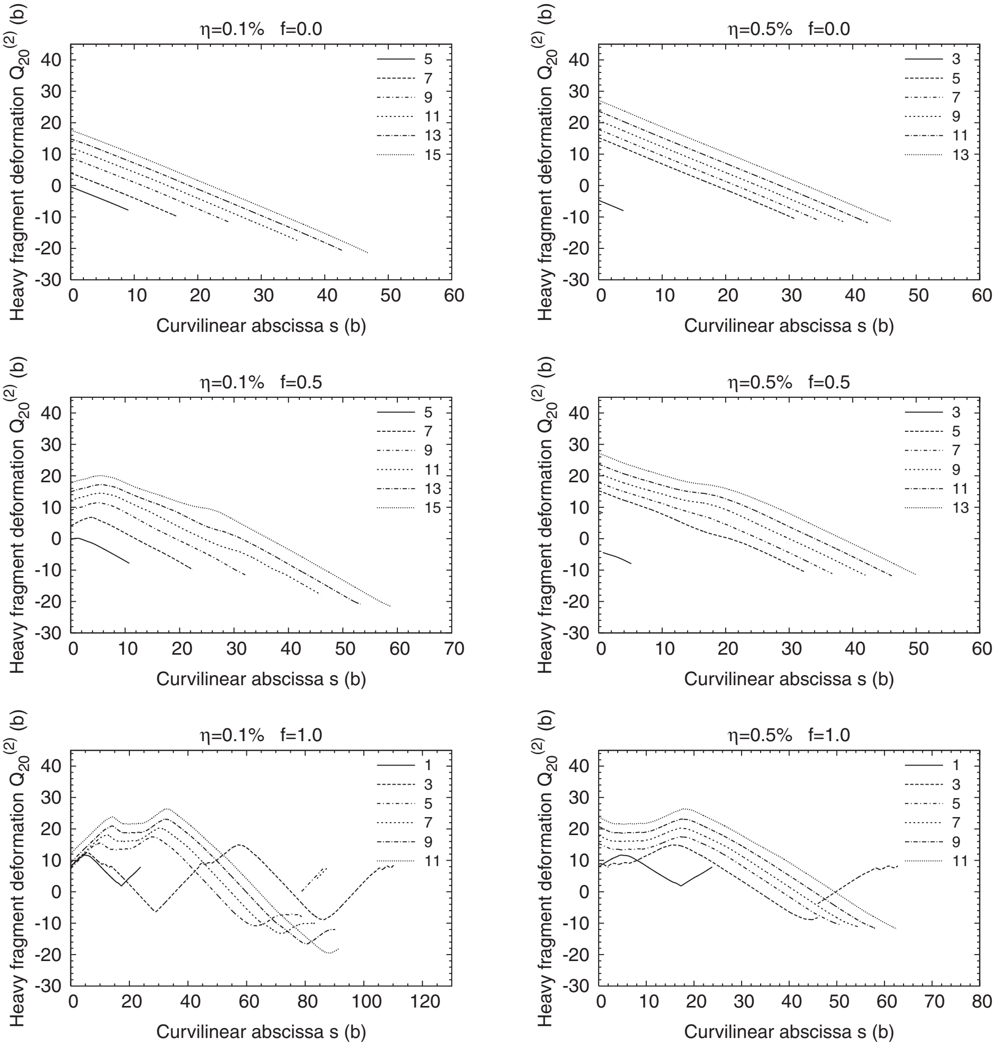

FIG. 8. Same as Fig. 6, but for the quadrupole moment of the heavy fragment $Q_{20}^{(2)}$.

two-dimensional (2D) representation turns out to be sufficient here. Indeed, from the scission condition given by Eq. (18), we can express $D_{\text{c.m.}}$ as a function of the fragment quadrupole moments, and as can be seen in Fig. 4, the contours of constant values of $D_{\text{c.m.}}$ as a function of the fragment deformations are almost straight lines parallel to each other. The surface representing the function $D_{\text{c.m.}}(Q_{20}^{(1)}, Q_{20}^{(2)})$ is therefore approximately a plane, especially in the ranges $Q_{20}^{(1)} \geqslant -10$ and $Q_{20}^{(2)} \geqslant -20$ b, which happen to correspond to the relevant regions of scission configurations (see next paragraph). We can therefore discuss the features of any contour $\mathcal{C}_{\text{TXE}}$ and the variation of quantities along this contour from the projection of $\mathcal{C}_{\text{TXE}}$ on the $(Q_{20}^{(1)}, Q_{20}^{(2)})$ plane.

The pattern of the TXE contours in the $(Q_{20}^{(1)}, Q_{20}^{(2)})$ plane explicitly depends on the actual values of η (ratio of nuclear and Coulomb interaction energies) and f (fraction of available energy at scission that goes into fragment kinetic energy). In this study, we retain two values of η based on the following qualitative arguments. On the one hand, the scission configurations selected by Eq. (18) must be such that the particle transfer between both fragments ceased, which corresponds to a vanishing neck radius. This imposes an upper limit on η. On the other hand, given the uncertainties on the Coulomb and nuclear interaction energies approximated as mentioned above, it is safer to discard η values leading to very small nuclear interaction energies (below, say, 0.5 MeV or so). We therefore retain the values 0.1% and 0.5% for η. As for f, we choose three values: the lower limit 0, the upper limit 1, and an intermediate value 0.5.

For the six combinations of η and f values, the lines of constant total excitation energy in the $(Q_{20}^{(1)}, Q_{20}^{(2)})$ plane are displayed in Fig. 5. We first notice a strong similarity between the contour diagrams for the same value of f and different values of η. This can be explained as follows. From Eq. (33), upon using Eq. (27) valid for small values of η, like the ones considered here, we deduce that

$$\begin{aligned}\text{TXE} \;=\; & f\sum_{i=1}^{2} E_{\text{def}}^{(i)}\big(Q_{20}^{(i)}\big) + (1-f)\big[Q - E_C\big(Q_{20}^{(1)},\\ & Q_{20}^{(2)}, D_{\text{c.m.}}\big(Q_{20}^{(1)}, Q_{20}^{(2)}\big)\big)\big],\end{aligned} \tag{41}$$

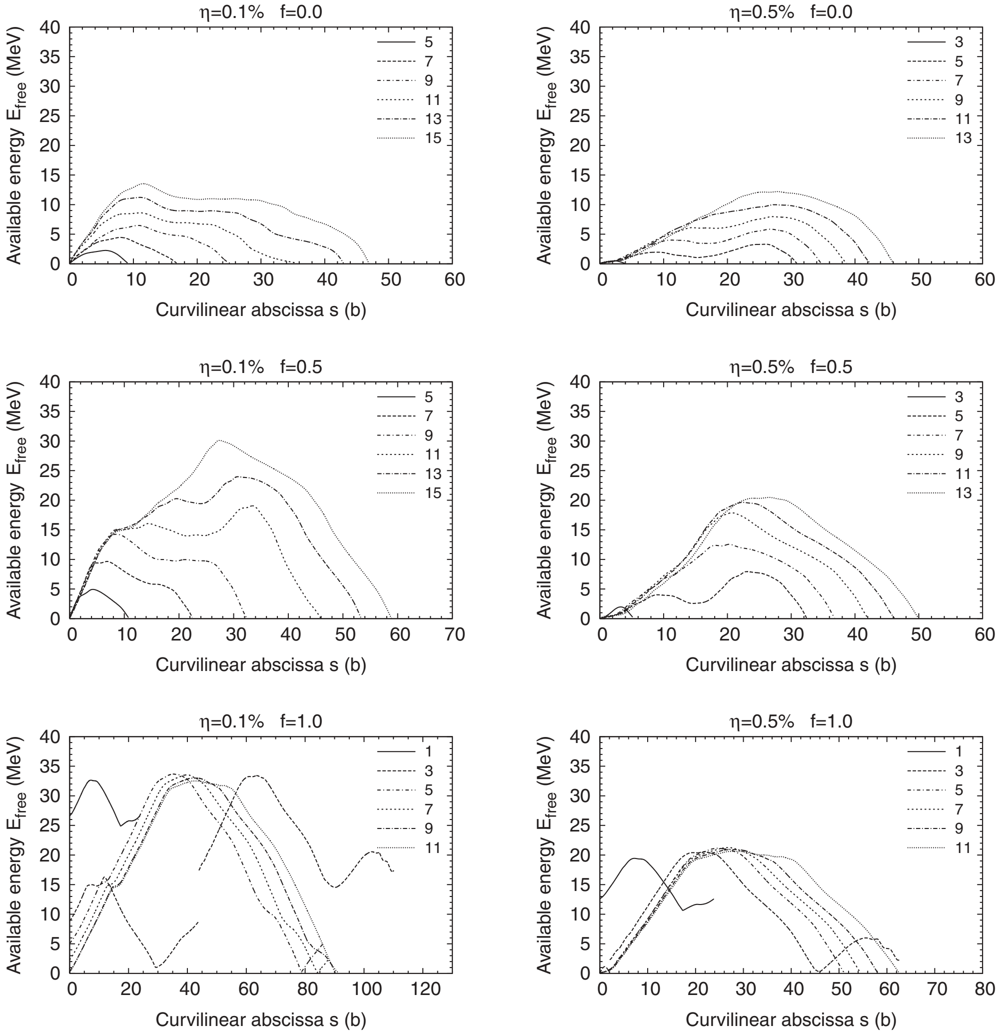

FIG. 9. Same as Fig. 6, but for the available energy at scission $E_{\rm free}$.

where $D_{\rm c.m.}$ varies slowly with η for fixed values of $Q_{20}^{(i)}$. Thus the contour diagram of TXE at a given value of f depends very little on η. The only visible pattern difference between contours in the left and right columns of Fig. 5 corresponding to the same f value is the deformation region covered by the scission configurations that Eq. (19) allows. To this difference should be added a shift in the values of TXE labeling the level contours, coming from a shift in E_C weakly dependent on the fragment deformations and induced by the difference in η values. This argument becomes exact when $f = 1$, since in that case, the total excitation energy of the fragments reduces to the sum of their deformation energies. In contrast, TXE strongly depends on f and varies from $E_{\rm def}^{(1)} + E_{\rm def}^{(2)}$ for $f = 1$ to $E_{\rm def}^{(1)} + E_{\rm def}^{(2)} + E_{\rm free}$ for $f = 0$. In the latter case, we can actually write TXE as $Q - E_C$, the nuclear interaction energy being neglected. Therefore, the total excitation energy is simply the opposite of the Coulomb interaction energy, up to a constant, which is the Q value of the spontaneous-fission reaction.

Finally, it is important to notice that some of the TXE contours are incomplete for two reasons. On the one hand the ends of the contours closer to the bottom left corner of the $(Q_{20}^{(1)}, Q_{20}^{(2)})$ box form a line separating the "excluded region," where no scission configurations are found, from the "scission region." On the other hand, some contours are interrupted because of the upper limits of the light- and heavy-fragment deformation ranges.

Our aim is to yield the variation of $\overline{J_f}$ as a function of TXE, thus combining the information given in Figs. 3 and 5. Considering one particular value of TXE means that we consider all points on an iso-TXE curve (as the curves corresponding to given values of TXE, η, and f in Fig. 5). Of course, all the points on such a curve are not on an equal footing.

For any such point, the energy at scission $E_{\rm sc}$ given by Eq. (20) defines the probability of reaching this point during the fission process. As stated at the end of the previous section, we mock up the distribution of quantal shape fluctuations by a Gaussian law in the single effective deformation variable s of Eq. (35), which is a sound approximation only in the case of a single well-defined minimum of $E_{\rm sc}$. In many instances, this is hardly the case, as exemplified in Fig. 6, giving $E_{\rm sc}$ as a function of s for various η, f, and TXE values.

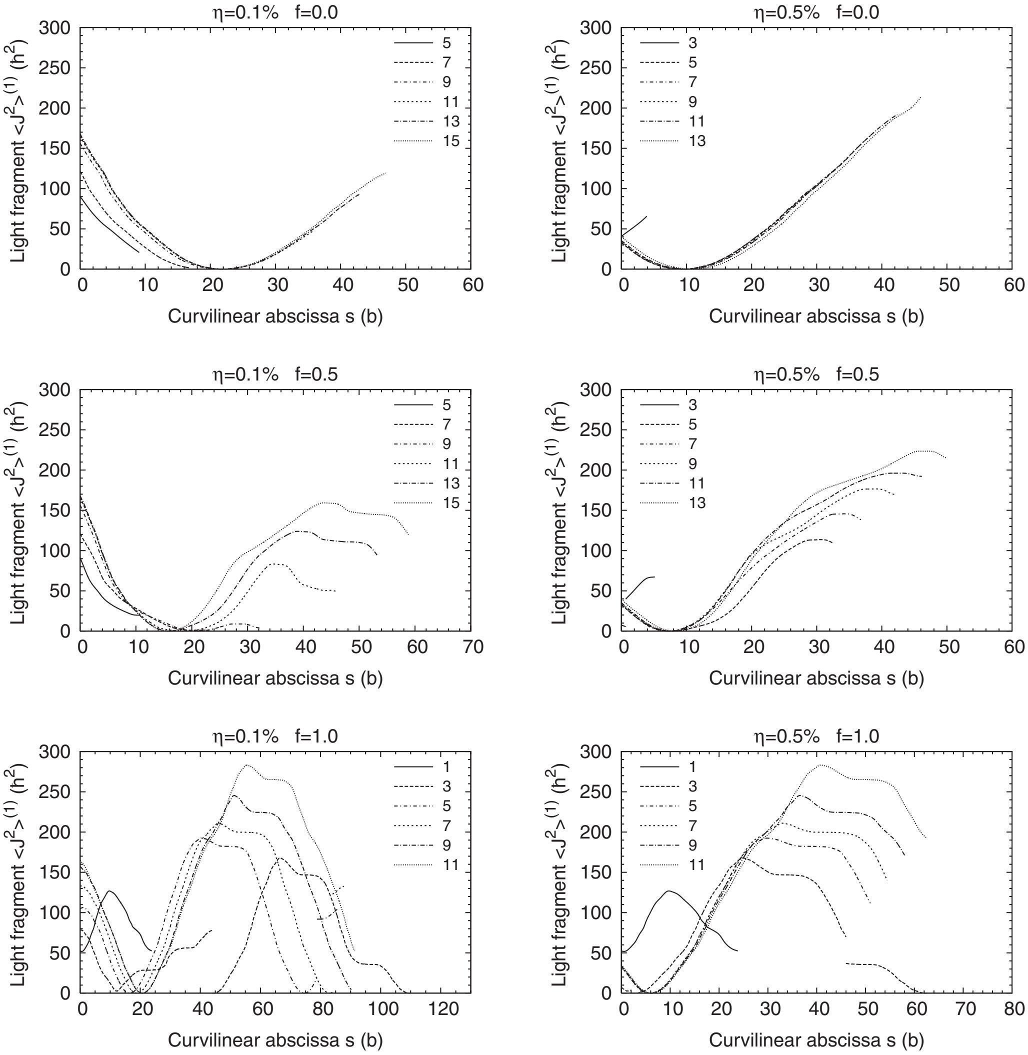

FIG. 10. Same as Fig. 6, but for the expectation value of $\hat{\mathbf{J}}^2$ of the light fragment $\langle J_1^2\rangle_{\text{intr}}$.

The width of this distribution is assumed to be fixed once and for all. The maximum of the probability (or the minimum of E_{sc}) is noted on the iso-TXE curves by a dot. For $f \neq 0$, above some critical value of TXE, the retained 2D deformation space is not large enough to accommodate very large prolate deformations of the heavy fragment which would be needed to reach the minimum of E_{sc}. As a result, in these cases, we omit the corresponding high values of TXE in the discussion of the results on the fission-fragment spins below.

Table II gives the maximal value of TXE for which the corresponding contour $\mathcal{C}_{\text{TXE}}$ is considered as complete, i.e., for which the ends are "physical" or for which the above probability distribution at the ends is so small that the integral of Eq. (37) is not affected by the missing part of $\mathcal{C}_{\text{TXE}}$.

Let us now discuss the location in the $(Q_{20}^{(1)}, Q_{20}^{(2)})$ plane of the most probable scission configuration (indicated by a dot) as a function of TXE for the different values of η and f. To do so we note that, using Eq. (41) and neglecting E_N in Eq. (20), the scission-configuration energy E_{sc} for a fixed TXE value varies with the curvilinear abscissa s along the iso-TXE contour as

$$E_{\text{sc}}(s) = \begin{cases} \dfrac{1}{1-f}\displaystyle\sum_{i=1}^{2} E_{\text{def}}^{(i)}\big(Q_{20}^{(i)}(s)\big) + E_{\text{GS}} - \dfrac{\text{TXE}}{1-f} & \text{if } f \neq 1, \\ E_C\big(Q_{20}^{(1)}(s),\quad Q_{20}^{(2)}(s),\, D_{\text{c.m.}}(s)\big) & \\ \quad + \text{TXE} + \displaystyle\sum_{i=1}^{2} E_i^{(\text{GS})}\big(Q_{20}^{(i)}(s)\big) & \text{if } f = 1. \end{cases} \tag{42}$$

TABLE II. Maximal value of TXE (in MeV) for which the contour $\mathcal{C}_{\text{TXE}}$ is considered as complete, for the six combinations of η and f values.

	TXE$_{\text{max}}$		
	$f = 0$	$f = 0.5$	$f = 1$
$\eta = 0.1\%$	35	29	17
$\eta = 0.5\%$	23	23	17

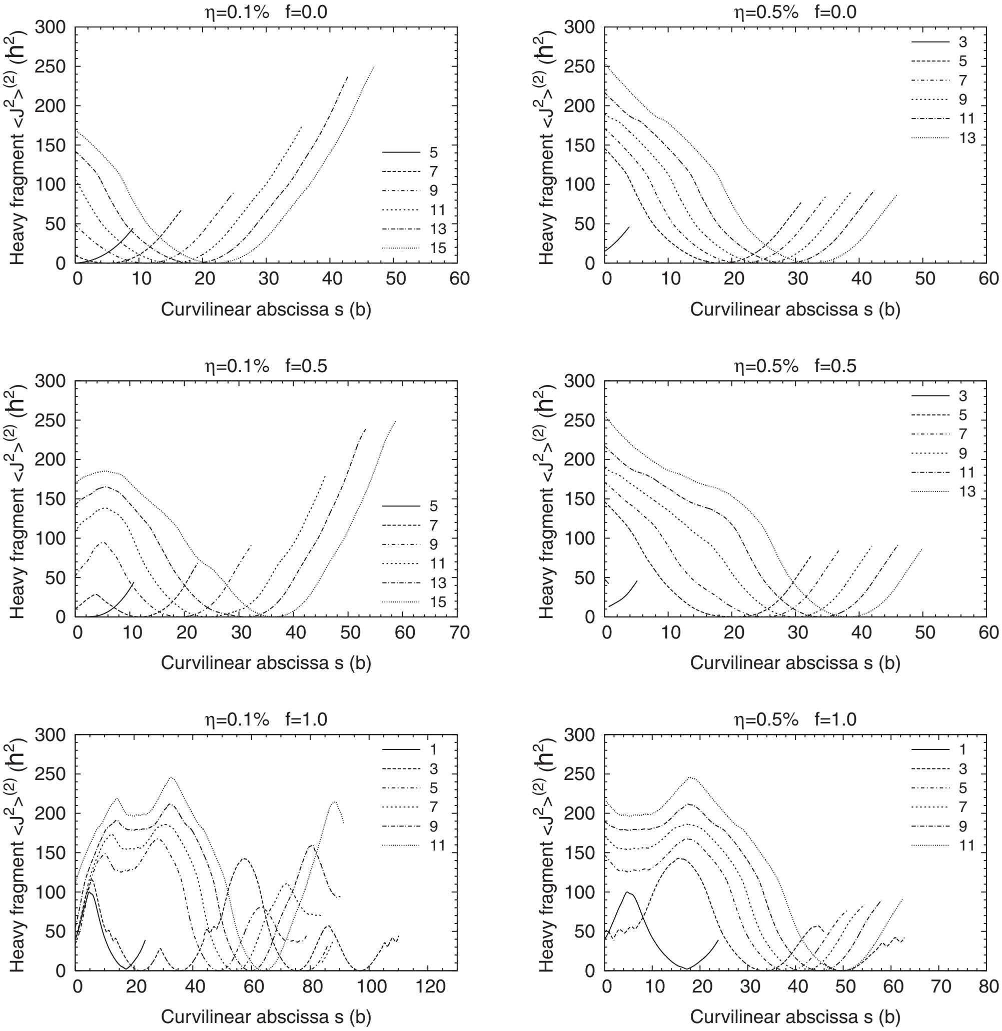

FIG. 11. Same as Fig. 10, but for the heavy fragment.

When $f \neq 1$, the most probable scission configuration therefore corresponds to the value of s that minimizes the total fragment deformation energy within the respective ranges $\mathcal{Q}_1(\text{TXE})$ and $\mathcal{Q}_2(\text{TXE})$ of $Q_{20}^{(1)}$ and $Q_{20}^{(2)}$ that generate the iso-TXE contour. For given η, f, and TXE values, let us denote the abscissa of the minimum of $E_{\text{sc}}(s)$ by s_0, as exhibited in Fig. 6. The coordinates in the $(Q_{20}^{(1)}, Q_{20}^{(2)})$ plane of the dot marking the most probable scission configuration on the corresponding TXE contour are therefore $Q_{20}^{(1)}(s_0)$ and $Q_{20}^{(2)}(s_0)$ and can be read in Figs. 7 and 8 representing the variations of the light- and heavy-fragment quadrupole moments, respectively, as functions of s for the six pairs of η and f values.

A striking feature of the variation of the dot locations in the $(Q_{20}^{(1)}, Q_{20}^{(2)})$ plane is a sudden jump from $Q_{20}^{(1)} \approx -5$, $Q_{20}^{(2)} \approx 11$ b to $Q_{20}^{(1)} \approx 8$, $Q_{20}^{(2)} \approx -5$ b for $\eta = 0.1\%$ and $f \neq 1$. This is explained by the transition from the low-s minimum corresponding to an oblate light fragment and prolate heavy fragment to the deeper, large-s minimum corresponding to the opposite situation (see Figs. 7 and 8). The reason for this behavior is to be found in the softness of the heavy fragment and the existence of two local minima along the light-fragment deformation-energy curve. To illustrate this, let us take the example of the contour map obtained with $\eta = 0.1\%$ and $f = 0.5$ (middle panel of the left column of Fig. 5). The deformation energy of the heavy fragment $E_{\text{def}}^{(2)}$ varies slowly in the ranges $\mathcal{Q}_2(\text{TXE})$ associated with TXE values lower than about 10 MeV. Therefore, the location of the most probable scission configuration is virtually only determined by the light-fragment deformation $Q_{20}^{(1)}$ that minimizes $E_{\text{def}}^{(1)}$ in the range $\mathcal{Q}_1(\text{TXE})$. For $\text{TXE} \leqslant 10$ MeV, the iso-TXE curves are confined in a rectangle such that $Q_{20}^{(1)} < q_1$, where $q_1 \approx 7$ b is the light-fragment quadrupole moment lying between the two local minima of the ^{106}Mo deformation-energy curve ($q_1^{(\text{obl})}$ on the oblate side and $q_1^{(\text{prol})}$ on the prolate side), and for which the deformation energy equals that of the oblate minimum: $E_{\text{def}}^{(1)}(q_1) = E_{\text{def}}^{(1)}(q_1^{(\text{obl})})$. As a result, for $\text{TXE} \leqslant 10$ MeV, the most probable scission configuration corresponds to the point of $\mathcal{C}_{\text{TXE}}$ whose abscissa is $Q_{20}^{(1)} = q_1^{(\text{obl})}$. Between $\text{TXE} = 11$ and $\text{TXE} = 15$ MeV, a similar situation on the prolate side of the light-fragment deformation-energy curve

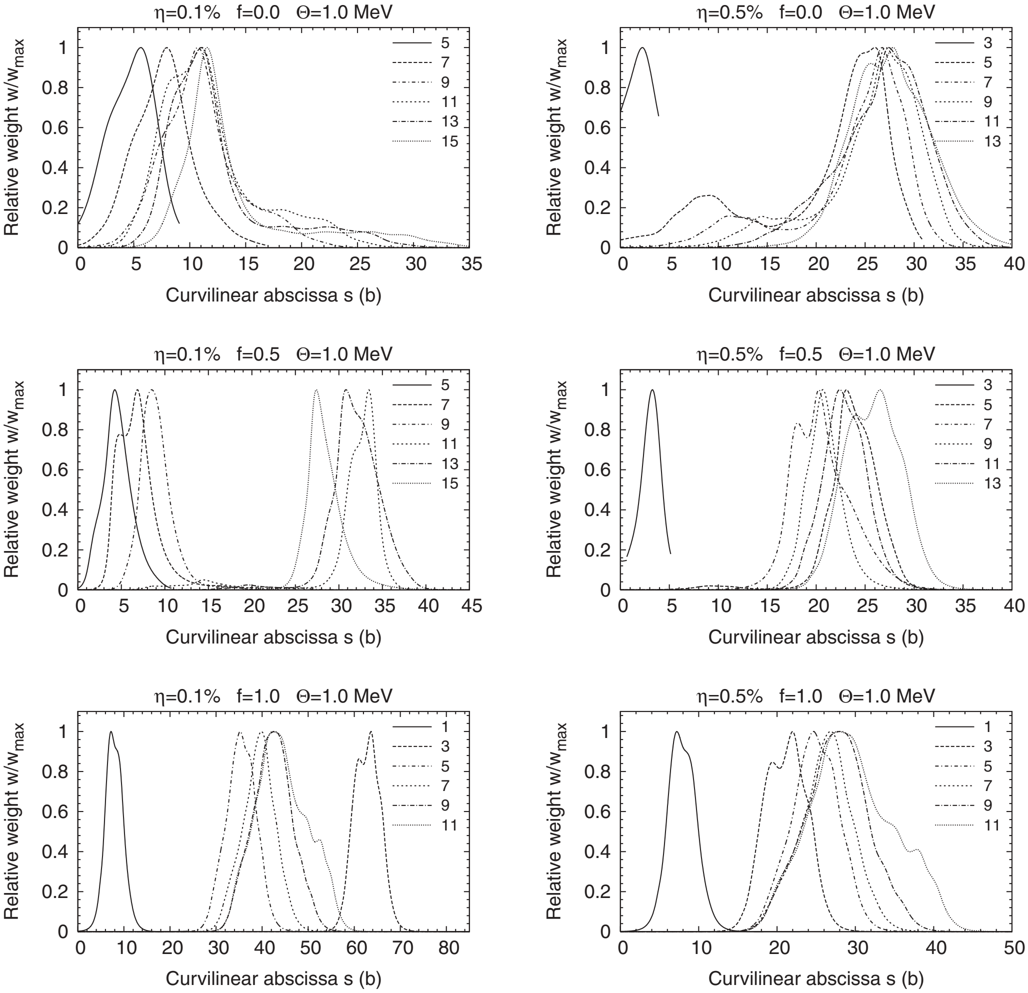

FIG. 12. Same as Fig. 6, but for the scission configuration probability w with $\Theta = 1$ MeV.

gives the same pattern for the sequence of dots on TXE contours with an approximately constant abscissa $Q_{20}^{(1)} \approx q_1^{(\mathrm{prol})}$. Above TXE = 16 MeV, the actual deformations minimizing the sum $E_{\mathrm{def}}^{(1)} + E_{\mathrm{def}}^{(2)}$ result from a subtle balance between the energy costs arising from letting the fragments depart from their lowest energy configurations among all those allowed for the considered value of TXE.

To close this subsection, let us focus on two other properties varying along the TXE contours, namely, the available energy at scission E_{free} plotted in Fig. 9 and the angular-momentum content (fragment expectation value of $\hat{\mathbf{J}}^2$) represented in Figs. 10 and 11 for the different values of η and f.

From Eqs. (24) and (23) we can deduce that $E_{\mathrm{free}}(s)$ is related to $E_{\mathrm{sc}}(s)$ in a very simple way;

$$E_{\mathrm{free}}(s) = -E_{\mathrm{sc}}(s) + E_{\mathrm{GS}}. \tag{43}$$

This relation reflects the meaning of E_{free}: the lower the scission configuration lies with respect to the ground state of the fissioning nucleus, the more energy is available to the fragments, shared in kinetic energy E_K or intrinsic energy E_{intr}. An interesting feature of the curves of $E_{\mathrm{free}}(s)$ is the increasing maximum value reached for successive TXE values when $f \neq 1$. In contrast, when $f = 1$, the maximum of the curves is virtually independent of TXE. This feature, combined with the location of the most probable scission configuration on a given TXE contour, will be used to explain the variation of the average available energy with TXE in the next subsection.

As for the variations of $\langle\hat{\mathbf{J}}^2\rangle^{(i)}$ with s, the patterns of the corresponding curves differ significantly for the light and heavy fragments. However, for both fragments, $\langle\hat{\mathbf{J}}^2\rangle^{(i)}(s)$ vanishes at the same value of $Q_{20}^{(i)}$ for $9 \leqslant \mathrm{TXE} \leqslant 17$ MeV when $f \neq 1$. Moreover, the variation of $\langle\hat{\mathbf{J}}^2\rangle^{(2)}(s)$ for different TXE values does not change much when going from $f = 0$ to $f = 0.5$ (for both values of η). In contrast, a smooth dispersion of the curves is observed for the light fragment when increasing f from 0 to 1: the maximum of each curve increases with TXE more and more as f increases. Finally, a common feature of the $\langle\hat{\mathbf{J}}^2\rangle^{(i)}(s)$ curves corresponding to a given TXE value for both fragments is that they reach higher values when $f = 1$, regardless of the value of η. We therefore expect higher average (taken over s) values of J_f for $f = 1$ than for $f \neq 1$, as will be discussed in the end of the next subsection.

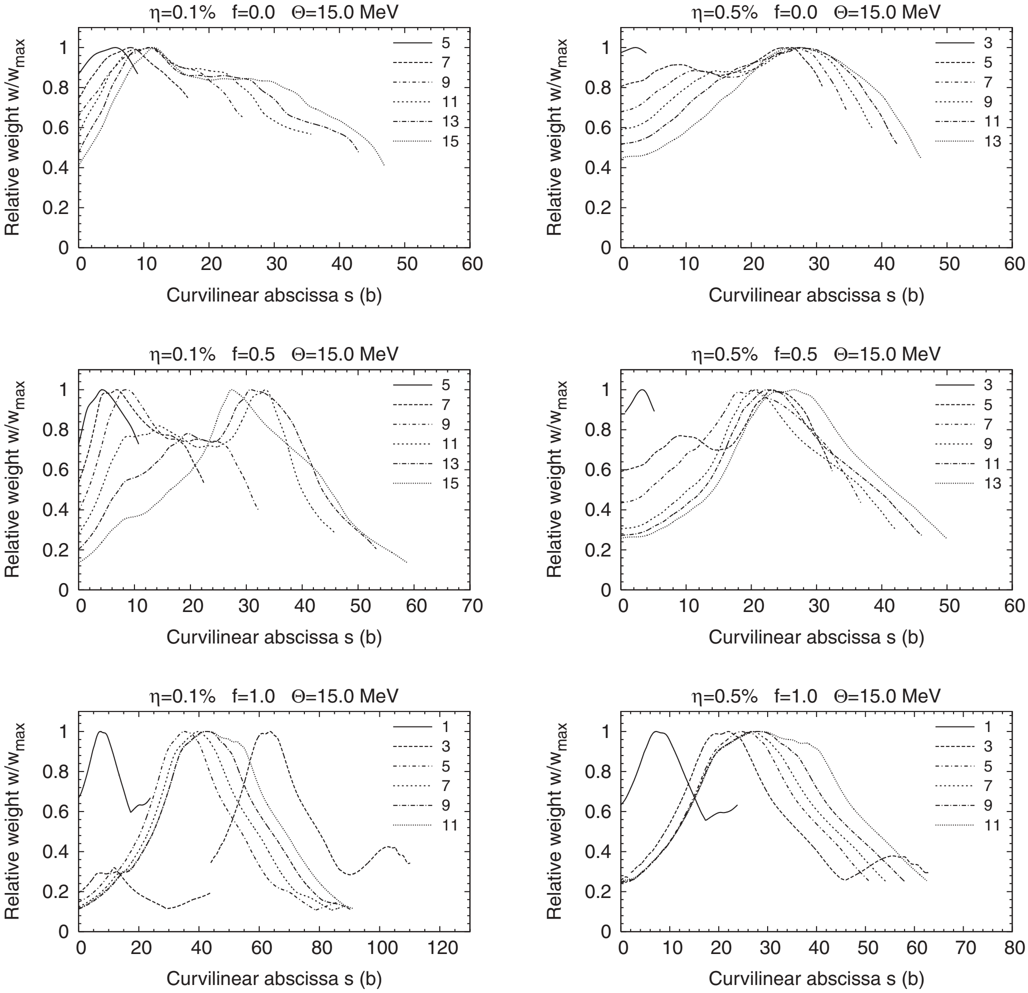

FIG. 13. Same as Fig. 12, but with $\Theta = 15$ MeV.

C. Average values

Upon leaning on the scission-point properties presented and discussed earlier, we can now focus on their average at given values of TXE. Figures 12 and 13 display, for the two considered values of the collective-energy parameter Θ (1 and 15 MeV), the distribution in s on selected constant-TXE contours for each pair of η and f values. For the sake of clarity, these distributions have all been scaled so that the highest probability is normalized to unity. Let us discuss first the results obtained with $\Theta = 1$ MeV and $\eta = 0.1\%$. For $f = 0$, we observe a smooth shift of the probability distributions toward higher values of s upon increasing TXE. This reflects the pattern of the scission-configuration energy curve $E_{\mathrm{sc}}(s)$ as a function of TXE shown in Fig. 6. In a similar way, for $f = 0.5$, the sudden shift of the peak of the distribution from low s values to larger ones when increasing TXE from 9 to 13 MeV results from the behavior of E_{sc}. This is correlated with a transition in the most probable configuration from an oblate deformation of the light fragment to a prolate one, as seen in Fig. 5. For $f = 1$ the same phenomenon occurs at a much lower value of TXE (between 1 and 5 MeV). The smoother behavior of E_{sc} for $\eta = 0.5$, visible in Fig. 6, mirrors itself in a smoother transition toward larger s values of the probability distributions in Fig. 12.

As seen in Fig. 13, the probability distribution functions obtained with $\Theta = 15$ MeV are rather spread out over large ranges of s values, with the noticeable exception of the curves obtained with the lowest TXE value for each set of η and f values. This exception is consistent with the fact that the region of the $(Q_{20}^{(1)}, Q_{20}^{(2)})$ plane available at these values of TXE is very limited. This may be easily understood again upon inspecting the behavior of E_{sc} in Fig. 6. Indeed, at the scale of a zero-point energy of the order of 1 MeV, the scission-configuration distribution is sensitive to shallow local minima, which is obviously not the case at an energy scale of 15 MeV.

Now, we have to decide which distribution width Θ is the most appropriate to our particular problem. The key to answering this question is related to the validity of the Born-Oppenheimer approximation [62] which is at the root of our description of scission points. In other words, we must make sure that Θ, which represents a typical collective energy E_{coll} in a mode involving the variable s, yields a characteristic time T for this motion that is fast with respect to, e.g., a characteristic time T_f for the descent from saddle to scission. In a harmonic case boldly invoked here for the sake of definiteness, T would represent the period and $E_{\rm coll}$ the phonon energy, quantities which are related by

$$T(\mathrm{s}) = \frac{4.1 \times 10^{-21}}{E_{\rm coll}(\mathrm{MeV})}. \tag{44}$$

If we retain for the characteristic fission time $T_f = 10^{-21}$ s (see, e.g., Ref. [63]), then

$$E_{\rm coll} \gg 4 \text{ MeV}. \tag{45}$$

Since $E_{\rm coll}$ is associated with twice the zero-point motion energy, we are led, in this harmonic approximation, to impose that

$$\Theta \gg 2 \text{ MeV}. \tag{46}$$

This entails that in the following, we will mostly discuss the averaged results with $\Theta = 15$ MeV. The value of $\Theta = 1$ MeV retained in Ref. [56] could be deemed as somewhat reasonable if it represented a temperature (essentially for the collective modes). However, the existence of an underlying equilibrium is to be justified, in particular because the authors of Ref. [56] define their scission points much earlier in the fission process than we do (for the values of η which we have retained). Indeed, they define the scission point for a fixed tip distance of 1.4 fm where the rupture of the neck has not yet occurred, in view of the nuclear diffuseness. For a pure Fermi density distribution with the diffuseness parameter of Ref. [64], we obtain 21% of the equilibrium nuclear matter density at half the considered tip distance. With such a simply connected nuclear shape, it is likely that the elongation and fragment deformation modes are still strongly coupled dynamically and not thermally. We therefore stand by our interpretation of Θ as depicting quantal fluctuations, for which the value $\Theta = 15$ MeV seems thus more appropriate than $\Theta = 1$ MeV.

Before discussing in the next subsection the values of the fission-fragment angular momenta resulting, at a given TXE value, from the average over s of all scission configurations (with $\Theta = 15$ MeV), we need to comment on some other average properties of the scission points. This leads us to describing in a broader way the scission-point properties obtained within our model assumptions. Clearly, this information would be relevant to studies whose scopes are much more extended than the mere description of fission-fragment spins.

The first quantities discussed here are the free ($E_{\rm free}$) and deformation ($E_{\rm def} = E_{\rm def}^{(1)} + E_{\rm def}^{(2)}$) energies. At a given point in the ($Q_{20}^{(1)}, Q_{20}^{(2)}$) plane, they do not depend, obviously, on f or Θ. Nevertheless, their average value at a given TXE does. As for the dependence on f, it comes from the integration contour $\mathcal{C}_{\rm TXE}$ in a very similar way as that encountered in Eq. (35). The results are displayed in Fig. 14 for $E_{\rm free}$ and Fig. 15 for $E_{\rm def}$. When going from $\eta = 0.5\%$ to $\eta = 0.1\%$, the global trends of both curves (as functions of TXE) are almost conserved. Since changing the value of η in this way moves the scission point away from the saddle point in the fission process, it is easy to understand why the values of $E_{\rm free}$ increase. Their dependence on TXE results from the averaging process and is difficult to trace back to any simple dynamical source. For $f = 0$, the

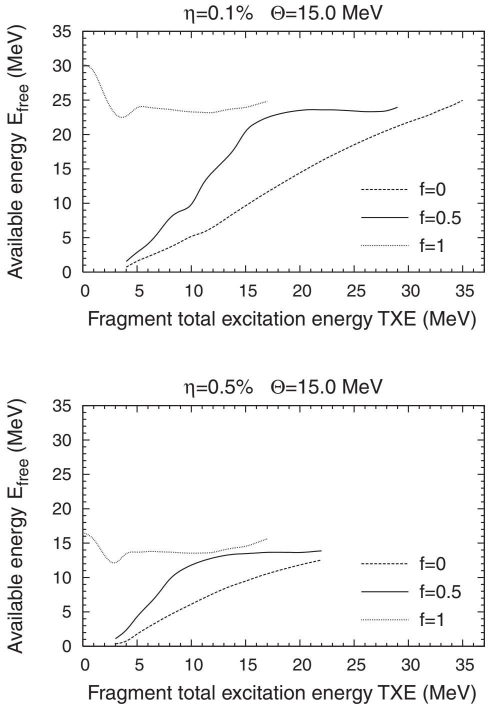

FIG. 14. Available energy at scission $E_{\rm free}$ as a function of the fragment total excitation energy TXE for $\eta = 0.1\%$ and $\eta = 0.5\%$. Results are shown for $\Theta = 15$ MeV only.

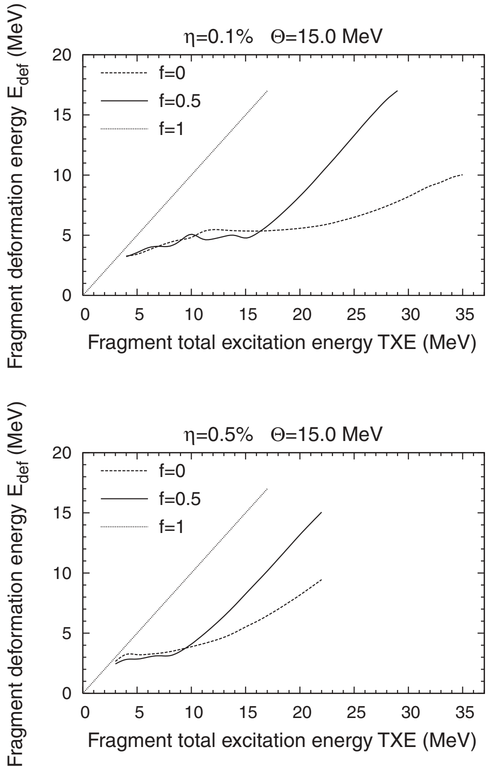

FIG. 15. Same as Fig. 14, but for the total energy of deformation of the fragments $E_{\rm def}$.

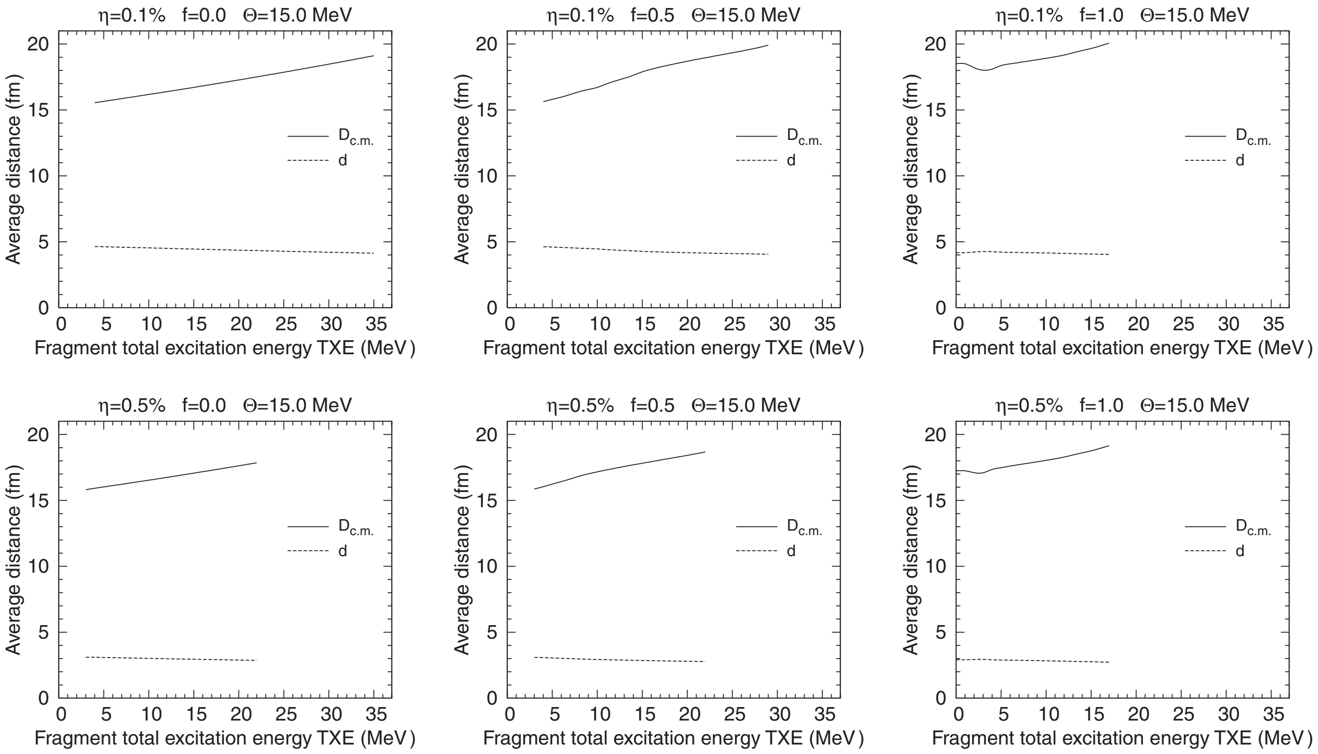

FIG. 16. Same as Fig. 14, but for the center-of-mass distance $D_{\mathrm{c.m.}}$ and the tip distance d.

variation of E_{def} is correlated to the one of E_{free}, since in that case their sum equals TXE. In the other limiting case ($f = 1$), TXE is exactly equal to E_{def}.

Let us now discuss the compactness of the fissioning system at scission through the variation of two important quantities in this respect, namely, the center-of-mass distance $D_{\mathrm{c.m.}}$ and the tip distance d. As shown in Fig. 16, the former varies much more with TXE than the latter. Indeed, the steady increase of average $D_{\mathrm{c.m.}}$ with TXE is rather closely connected with the decrease in TKE whose largest part is the mutual Coulomb energy roughly varying as $1/D_{\mathrm{c.m.}}$ (see next paragraph for a more detailed discussion). On the other hand, the tip distance shows a consistent but small decrease as TXE gets larger. It is difficult to come up with a simple explanation for this, because one has to disentangle the balancing effects (upon increasing TXE) of a consistent drift of average shapes in both fragments and an increase of $D_{\mathrm{c.m.}}$ under the constraints of fixed values of TXE and η.

The last important average scission-point quantity is the variation of TKE with the center-of-mass distance displayed in Fig. 17. In the $f = 0$ case, where there is no prescission component coming from E_{free}, the fragment total kinetic energy is simply equal to the Coulomb mutual energy at scission, and it is interesting to compare it with what would result from a pure monopole-monopole interaction of the $Z_1 Z_2/D_{\mathrm{c.m.}}$ type. As seen in Fig. 17, there is a slight variation which can be readily connected with the next term in the multipole-multipole expansion of the Coulomb interaction. Indeed, for instance in the $\eta = 0.1\%$ case, as $D_{\mathrm{c.m.}}$ increases, i.e., as TXE gets larger, one goes from an oblate-oblate average configuration toward a spherical-prolate one, passing through a region of oblate-prolate shapes. Therefore, one experiences a transition from configurations yielding a negative quadrupole correction to the monopole Coulomb interaction to configurations allowing a positive correction, passing through a region of a vanishing quadrupole contribution. For other values of f (0.5 and 1), the connection between $D_{\mathrm{c.m.}}$ and TKE is less clear, but the general trends are quite similar.

D. Fission-fragment angular momenta

We come finally to the results of fission-fragment angular momenta. For each considered TXE value, they were obtained by averaging J_f over the scission configurations lying on the corresponding path $\mathcal{C}_{\mathrm{TXE}}$. In this way, we obtain the curves $\overline{J_f}(\mathrm{TXE})$ displayed in Fig. 18 with $\eta = 0.1\%$ and $\eta = 0.5\%$.

Before comparing these results with experimental data, we want to comment on the variation of $\overline{J_f}$ with TXE. First of all, in the $f = 1$ case, the curves $\overline{J_f}(\mathrm{TXE})$ are found to be somewhat dependent on the specific value of η. The total fragment excitation energy reduces here to the total deformation energy of the fragments E_{def} whose functional dependence on $Q_{20}^{(1)}$ and $Q_{20}^{(1)}$ is independent of η. As can be seen in Figs. 8, 9, and 13, both the integration contours and the averaging weights are similar for $\eta = 0.1\%$ and $\eta = 0.5\%$.

Next, let us compare for both values of η the relative position of the $\overline{J_f}(\mathrm{TXE})$ curves associated with different values of f. As f gets larger, the increase of J_f becomes faster. This is to be correlated with the results presented in Fig. 14 showing that for both values of η, the deformation energy E_{def} increases more rapidly as f gets larger. Of course, in general, a rise in the deformation energies does not mean that the deformation

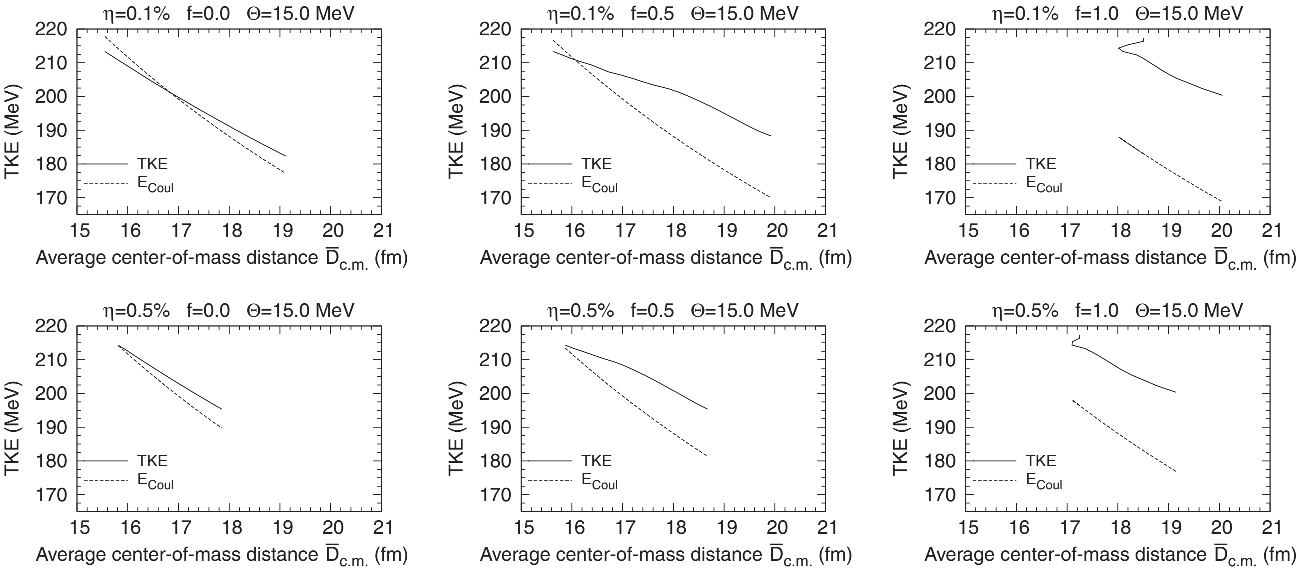

FIG. 17. Variation of total kinetic energy of the fragments TKE as a function of the average center-of-mass distance $\overline{D}_{\text{c.m.}}$ for the six combinations of η and f values.

increases. But owing to the rather shallow character of the local equilibrium wells evidenced in the PES displayed in Fig. 1, one may infer that above a few MeV, the increase in E_{def} implies that the deformations, hence the resulting spins, do increase.

Moreover, for all considered values of parameters η and f, with the collective-energy parameter $\Theta = 15$ MeV, we observe the overall trend that over the whole span of TXE values presented in Fig. 18, the fragment spin J_f is an increasing function of TXE. Nevertheless, we note as an exception a well-marked dip at low TXE values (typically below 5 MeV). Let us explain these facts in the representative case where $\eta = 0.1\%$ and $f = 0.5$ (dashed curve in the upper panel of Fig. 18). As TXE gets higher, we can see in Fig. 5, taking as a guide to the eye the dots indicating the deformation points of lowest E_{sc} value, that the fragments are initially fairly deformed, hence there is a finite, sizable value of $\overline{J_f}$. Then between 5 and 6 MeV, one crosses the spherical point of the heavy fragment, while the light fragment keeps a constant oblate deformation. This explains the very low value of $\overline{J_f}$ between 5 and 6 MeV. For TXE increasing up to 8 MeV, the light fragment keeps its oblate deformation, but the heavy fragment becomes more and more deformed (prolate), which leads to the increase of the spin between 6 and 8 MeV. Between 11 and 15 MeV, the most probable configuration implies a prolate light fragment, with a fairly constant quadrupole moment of about 10 b, while the heavy-fragment quadrupole moment gradually increases from about −5 to 10 b. In this excitation-energy range, the average spin varies in the same way as between 4 and 8 MeV. Finally, beyond 15 MeV, the heavy fragment becomes more and more prolate-deformed (actually both fragments between 16 and 21 MeV) and dominates the net variation of $\overline{J_f}(\text{TXE})$.

The same argument may be presented from another point of view. The variation of the intrinsic expectation values of $\langle \hat{\mathbf{J}}^2 \rangle_{\text{int}}$ for both fragments as functions of the curvilinear abscissa s is displayed in Figs. 10 and 11. Combining this information with the distribution patterns of Fig. 12 (again, for instance, in the $\eta = 0.1\%$, $f = 0.5$ case), we find that for low values of TXE (4–5 MeV), the most probable value of s increases

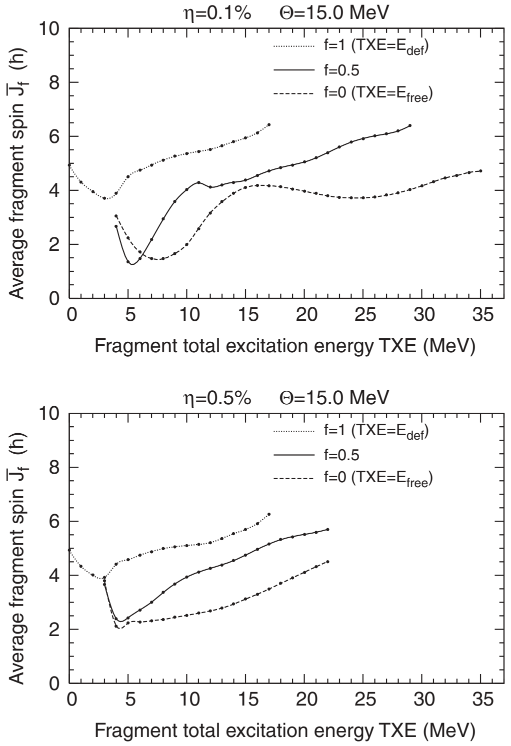

FIG. 18. Variation of average angular momentum in units of $\hbar$ at scission with the total excitation energy for the $^{106}\text{Mo}+^{146}\text{Ba}$ fragmentation. Dots mark the actual calculated results, curves serve to guide the eye.

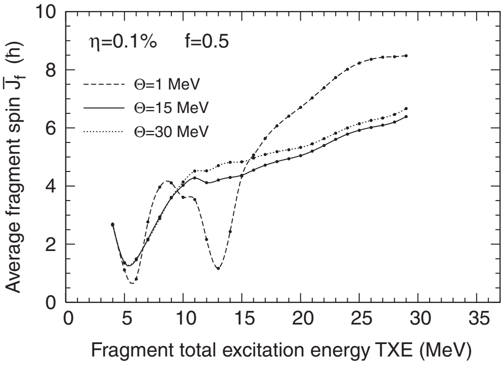

FIG. 19. Same as Fig. 18, but for different values of Θ with $\eta = 0.1\%$ and $f = 0.5$.

with TXE in a region of a marked decrease of $\langle \hat{\mathbf{J}}^2 \rangle_{\text{int}}$ with s for both fragments. At higher TXE values, the same increase of the most probable value of s occurs in a region where the above $\langle \hat{\mathbf{J}}^2 \rangle_{\text{int}}$ expectation values are increasing with s.

Finally, because some authors (as, e.g., Wilkins and collaborators [56]) made use of a different Θ value (1 MeV) and because of the arbitrary character of the preferred value of Θ even though it clearly satisfies the Born-Oppenheimer condition in Eq. (44), we perform in one particular case ($\eta = 0.1\%$ and $f = 0.5$) the averaging for a choice of three different values of Θ (1, 15, and 30 MeV). The corresponding results displayed in Fig. 19 may be interpreted in the following way. At low TXE values, the region of the $(Q_{20}^{(1)}, Q_{20}^{(2)})$ plane spanned by the allowed scission configurations is so limited that the probability distribution w given by Eq. (36) takes the same values for the different values of Θ, hence the independence of $\overline{J_f}$ with respect to Θ. As a consequence, the previously described decrease of $\overline{J_f}$ is found irrespective of any choice of Θ values. In contrast, the available fragment-deformation range gets larger as Θ increases. As expected then, upon using small values of Θ, one emphasizes the importance of local minima in $E_{\text{sc}}(s)$, which thus creates some fluctuations in the curves of $\overline{J_f}$ as a function of TXE, arising from minute variations of $E_{\text{sc}}(s)$ when changing TXE. On the other hand, comparing the results obtained with $\Theta = 15$ and 30 MeV, one finds almost no differences. This justifies *a posteriori* the choice of $\Theta = 15$ MeV, which is the value retained in the discussion of the next subsection.

E. Discussion of results

As apparent from the previous presentation, our results are understandably contingent upon a retained value of the parameter f specifying the partitioning of E_{free}. An exact value of it is very difficult to assess experimentally. However, the author of the pioneering work of Ref. [65] gave an estimate of the fraction $E_{\text{diss}}/\Delta V$ of the energy release ΔV between saddle and scission that is dissipated in fragment excitation energy E_{diss}. This ratio is simply related to our f parameter through $f = 1 - E_{\text{diss}}/\Delta V$. This estimate given by Gönnenwein [65] is based on a combinatorial analysis of pair breaking to account for the odd-even staggering effect observed in nuclear-charge yields from thermal- and MeV-neutron-induced fission. More recently Rejmund *et al.* [66] repeated the analysis of odd-even staggering in charge yields within a statistical approach including within the BCS approach the pairing effects on the nuclear level density. These efforts indicate that $E_{\text{diss}}/\Delta V$ changes slightly with the fissility parameter (from ^{220}Th to ^{250}Cf) but do not agree on the variation. In the ^{252}Cf region, Gönnenwein [65] found a ratio $E_{\text{diss}}/\Delta V \approx 0.44 \pm 0.02$, whereas Rejmund *et al.* [66] obtained a lower value, $E_{\text{diss}}/\Delta V \approx 0.34 \pm 0.01$. In these analyses, the experimental data used are obtained for compound-nucleus excitation energies in the 5–10 MeV range. Given the uncertainties pertaining to the model-dependent character of these calculations and to the deficiency of the BCS description of weak pairing regimes encountered when pairs begin to be broken, we deem it as a reasonable approximation to retain the median value $f = 0.5$ for the discussion of our results.

From these results, two features can be singled out. First, for TXE $\geqslant$ 5 MeV, the average angular momenta of the fragments steadily increase. Irrespective of the retained value of η, we find a rate of increase of $\overline{J_f}$ that is typically of the order of $1\hbar$ when TXE increases by 5 MeV. This is slightly less on average than $1\hbar$ per emitted neutron. The second point which should be stressed is that at low TXE values (typically 5 MeV), the value of $\overline{J_f}$ is found in the $2\hbar$ range.

Both features are roughly consistent with the findings of Ref. [13]. As amply discussed, one should not attempt to go beyond such a qualitative comparison because of the limitations of the current experimental approach and the present theoretical estimate.

Since the average number of emitted neutrons $\overline{\nu}$ is about 4 for ^{252}Cf (see Ref. [67]), one can consider that the average value of TXE is about 25 MeV. The resulting $\overline{J_f}$ value obtained for $f = 0.5$ may be considered as slightly too small in view of the average J_f value found years ago in Ref. [5]. This would then give a hint that f should be closer to 1 than to 0. On the basis of the results of Fig. 17 this would correspond to a value of the prescission kinetic energy in the range of 10 (20) MeV for $\eta = 0.5\%$ (0.1%). Of course, one should take this estimate with all the caution requested by the approximate character of our current approach.

The last comment that can be made relates to the necessary choice for the parameter η. As we have already discussed, the acceptable range for η is bounded within two limits rather different in nature. The upper limit is imposed from the condition that after scission at the very least no nucleonic exchange should take place, which entails the vanishing of a neck between the two fragments. The lower boundary is imposed by the approximate character of our calculation of the mutual Coulomb and nuclear energies. Below some limit, typically of some 100 keV for the latter (some per thousand in η), such a crude approach does not allow one to expect sufficient accuracy for the definition of the scission points. Beyond these considerations, one should further add that the Born-Oppenheimer condition does not imply at all that a single value of η should be retained. One may very well expect that the scission points along a fission valley are distributed (see, e.g., the tunneling between a "fission" and a "fusion" valley advocated in Ref. [68]). In that case, one does not have to decide which value of η should be deemed as the most realistic one. Instead, some averaging over a distribution may be more relevant.

VIII. CONCLUSIONS

The primary goal of this paper is to contribute to a better theoretical understanding of the microscopic mechanism at work in the generation of angular momentum of fragments issuing from a fission at zero or low excitation energy. We have, first of all, drawn two lessons from a brief survey of available experimental data.

On the one hand, the related experimental findings when expressed in terms of angular momenta of primary fragments do not constitute, by any means, a raw material, but rather results yielded by a highly elaborated model-dependent treatment. As a consequence, it is reasonable to take them as rough indications of absolute values and, correlatively, to consider as more serious constraints on any theory their variation with some global parameter ruling the whole fission process (as, e.g., the total excitation energy of the fragments).

On the other hand, a significant amount of data on fission-fragment angular momenta has and still does come from the observation of the population of isomeric states. In such cases, we claim that neither the usual model-dependent processing of the data nor the above-discussed simplified version of the orientation-pumping mechanism is fit, without significant adaptation, to such a peculiar situation. The reason for it lies in the fact that the quasiparticle character of isomeric states makes their rotational properties vastly different from those of a ground-state band of a deformed even-even nucleus. Despite the truly fascinating character of such data, embodying the completely different nature of the mechanism at work, we nevertheless have to exclude them, for the time being, from the scope of our current limited theoretical investigation.

Bearing in mind these limitations, we then proceed to discuss existing theoretical accounts of such an angular-momentum generation which may be deemed as a rather intriguing phenomenon. Indeed, in fluid mechanical terms, it starts as a purely potential flow and ends up as a highly vortical one in the center-of-mass system. The main common characteristic of these models is that they rely on the thermal excitation of some relevant collective modes to generate angular momenta. It is our main contention that the major reason for the existence of such finite angular momenta does not lie primarily in thermal but rather in quantal fluctuations. The latter are clearly issuing from a relevant version of the Heisenberg principle for spatially polarized systems, giving rise to the so-called orientation-pumping mechanism. Our aim is thus to check whether, ruling out by hypothesis all other possibly concurring sources of angular momentum, we can explain from state-of-the-art microscopic calculations using effective nucleon-nucleon forces, the bulk of their experimental values and their observed trend as a function of the total excitation energy. The answer is clearly positive, resulting from a detailed study of a particular pair of primary fragments in the spontaneous fission of ^{252}Cf, namely ^{106}Mo+^{146}Ba.

We should stress that in performing such an investigation, we deliberately excluded any specific consideration of how the system gets its spatially polarized character, thereby avoiding the difficulties encountered in previous theoretical approaches. Therefore, we cannot claim that we have completed a full theoretical investigation of the process but rather that we searched for the basic quantum mechanical rules that should apply to the solution of any model relevant to that matter.

Nevertheless, in the process of doing so, we are induced to paying particular attention to the more general question of the quantitative definition of a scission point. The implications of our study of these scission-point configurations reach far beyond the mere problem of fission-fragment spins. They might serve as ingredients, among others, of a much wanted quantitative study of various fission distributions which are generally thought to be mostly determined by the scission configurations. Of course, a complete description of those distributions should clearly include a study of the yields of all possible fragment pairs. This subject is clearly not touched upon here, since it would imply the inclusion of an additional collective variable ruling the mass asymmetry, such as the total octupole moment.

While the orientation-pumping mechanism appears as a quite general consequence of the usual quantum mechanics, its present practical implementation involves various further approximations rendering the present work no more than an exploratory approach even within its general purpose. The next steps to take would include, for example, an adequate study of the projection of the fragment intrinsic wave functions as well as a proper account of shape fluctuations. In spite of all its deficiencies, the present work yielding a somewhat reasonable agreement with available data certainly provides incentive for undertaking such an ambitious program.

ACKNOWLEDGMENTS

We gratefully acknowledge many enlightening discussions with Pr. F. Gönnenwein. Ph.Q. thanks the Theoretical Division at LANL for the excellent working conditions extended to him during his numerous visits. I.N.M. acknowledges valuable support from the JINR-IN2P3 agreement (Collaboration 03-61). This research was supported by the U.S. Department of Energy under Contract No. W-7405-ENG-36, the IN2P3/CNRS, and the JINR.

APPENDIX A: QUANTUM ROTOR IN A POLARIZING FIELD

In the orientation-pumping model of Ref. [4], the distribution of fission fragments in angular momentum I is proportional to the square of amplitudes a_I, which are the overlaps of the wave function of the "polarized" state representing the collective motion within the deformed mean field, and the states of a free rotor with good angular-momentum quantum numbers I and $M = 0$ (M denoting the projection of the angular momentum on the quantization axis).

To calculate these amplitudes, let us first consider the model Hamiltonian

$$H = -\frac{\hbar^2}{2\mu}\left[\frac{1}{\sin\theta}\frac{\partial}{\partial\theta}\left(\sin\theta\frac{\partial}{\partial\theta}\right) + \frac{1}{\sin^2\theta}\frac{\partial^2}{\partial\varphi^2}\right] + V(\theta), \tag{A1}$$

with the following potential that modelizes the polarizing field

$$V(\theta) = \tfrac{1}{2}C\sin^2\theta. \tag{A2}$$

In Eqs. (A1) and (A2), the constants μ and C denote the inertia and rigidity parameters, respectively. The exact eigenfunctions of the Hamiltonian (A1) are called oblate spheroidal wave functions [69].

When the orientation in space of the fissioning system is well defined, the polarizing field $V(\theta)$ is strong, so the rigidity constant C is large, and the wave function of the polarized state $\Psi(\theta,\varphi)$ is expected to decrease rapidly with θ. As a result, Ψ is an eigenfunction of the Hamiltonian H in the small angle limit and satisfies the differential equation

$$\begin{aligned} -\frac{\hbar^2}{2\mu}\left[\frac{1}{\theta}\frac{\partial}{\partial\theta}\left(\theta\frac{\partial\Psi}{\partial\theta}\right) + \frac{1}{\theta^2}\frac{\partial^2\Psi}{\partial\varphi^2}\right] + \frac{1}{2}C\theta^2\Psi(\theta,\varphi) \\ = E\Psi(\theta,\varphi), \end{aligned} \tag{A3}$$

with the eigenvalue E. Equation (A3) is the Schrödinger equation of a 2D isotropic angular harmonic oscillator, whose exact eigenvalues and wave functions are given by [30]

$$E_{\mathrm{nm}} = (2n + |m| + 1)\hbar\,\omega, \tag{A4}$$

and

$$\Psi_{\mathrm{nm}}(\theta,\varphi) = N_{\mathrm{nm}}\eta^{|m|}L_n^{|m|}(\eta)e^{-\eta/2}e^{im\varphi}, \tag{A5}$$

with the notation

$$\eta = \left(\frac{\theta}{\theta_0}\right)^2, \tag{A6}$$

$$\theta_0 = \sqrt{\hbar}(\mu C)^{-1/4}. \tag{A7}$$

The oscillator frequency ω and the normalization factor N_{nm} are given by

$$\omega = \sqrt{\frac{C}{\mu}}, \tag{A8}$$

$$N_{\mathrm{nm}} = \frac{1}{\theta_0\sqrt{\pi n!(n+|m|)!}}, \tag{A9}$$

and $L_n^{|m|}$ denotes the associated Laguerre polynomial of degree n.

Here we are interested in the lowest energy solution Ψ_0 in the case where $m = 0$ and in presence of a strong polarizing field. The wave function $\Psi_0(\theta)$ is therefore a solution to the equation

$$-\frac{\hbar^2}{2\mu}\frac{1}{\theta}\frac{d}{d\theta}\left(\theta\frac{d\Psi_0}{d\theta}\right) + \frac{1}{2}C\theta^2\Psi_0(\theta) = E\Psi_0(\theta) \tag{A10}$$

and is given by

$$\Psi_0(\theta) = \frac{1}{\theta_0\sqrt{\pi}}e^{-\frac{\theta^2}{2\theta_0^2}}. \tag{A11}$$

Following Rasmussen and collaborators [30], we now expand Ψ_0 onto good angular-momentum states Y_ℓ^0 (corresponding to the spherical harmonics with $m = 0$)

$$\Psi_0(\theta) = \sum_{\ell=0}^{\infty} a_\ell Y_\ell^0(\theta), \tag{A12}$$

where the amplitudes a_ℓ are defined by

$$a_\ell = 2\pi\int_0^\pi d\theta\,\sin\theta Y_\ell^0(\theta)\Psi_0(\theta). \tag{A13}$$

Owing to the approximation (A11) and the smallness of θ_0, the range of θ values for which the integrand of Eq. (A13) is sizable is restricted to $[0;\theta_0]$. Thus we can use the small angle limit and extend the integration up to infinity in Eq. (A13). In this limit, the spherical harmonic Y_ℓ^0 satisfies the equation

$$-\frac{1}{\theta}\frac{d}{d\theta}\left(\theta\frac{dY_I^0}{d\theta}\right) = \ell(\ell+1)Y_\ell^0(\theta). \tag{A14}$$

With the substitutions $z = \sqrt{\ell(\ell+1)}\theta$ and $f(z) = Y_\ell^0(\theta)$, Eq. (A14) can be brought to the form

$$z^2\frac{d^2f}{dz^2} + z\frac{df}{dz} + z^2f(z) = 0, \tag{A15}$$

which is the differential equation satisfied by the zero-order Bessel function of the first kind $J_0(z)$. As a result, in the small angle limit the spherical harmonic $Y_\ell^0(\theta)$ is given by

$$Y_\ell^0(\theta) \approx \sqrt{\frac{2\ell+1}{4\pi}}J_0(\sqrt{\ell(\ell+1)}\theta), \tag{A16}$$

and the amplitude a_ℓ therefore takes the form

$$a_\ell \approx \frac{\sqrt{2\ell+1}}{\theta_0}\int_0^\infty d\theta\theta J_0(\sqrt{\ell(\ell+1)}\theta)e^{-\frac{\theta^2}{2\theta_0^2}}. \tag{A17}$$

The integral can be calculated analytically [see Eq. (11.4.29) of Ref. [69]], and we finally obtain

$$a_\ell \approx \theta_0\sqrt{2\ell+1}e^{-\frac{\theta_0^2}{2}\ell(\ell+1)}. \tag{A18}$$

The expectation value of the square of the angular-momentum operator $\hat{\mathbf{L}}^2$ in the ground state Ψ_0 (normalized to unity)

$$\langle\Psi_0|\hat{\mathbf{L}}^2|\Psi_0\rangle = \sum_{\ell=0}^{\infty}\ell(\ell+1)a_\ell^2 \tag{A19}$$

is approximately

$$\langle\Psi_0|\hat{\mathbf{L}}^2|\Psi_0\rangle \approx \theta_0^2\sum_{\ell=0}^{\infty}\ell(\ell+1)(2\ell+1)e^{-\theta_0^2\ell(\ell+1)} \tag{A20}$$

$$\approx \theta_0^2\int_0^{\infty} d\ell\,\ell(\ell+1)(2\ell+1)e^{-\theta_0^2\ell(\ell+1)}, \tag{A21}$$

where $\int_0^{\infty} d\ell\,\ell(\ell+1)(2\ell+1)e^{-\theta_0^2\ell(\ell+1)} = 1/\theta_0^4$, that is,

$$\langle\Psi_0|\hat{\mathbf{L}}^2|\Psi_0\rangle \approx \frac{1}{\theta_0^2}. \tag{A22}$$

The corresponding average value $\bar{\ell}$ of ℓ, such that $\langle\Psi_0|\hat{\mathbf{L}}^2|\Psi_0\rangle = \bar{\ell}(\bar{\ell}+1)$, is thus given by

$$\bar{\ell} = \frac{1}{2}\left(\sqrt{1+4\langle\Psi_0|\hat{\mathbf{L}}^2|\Psi_0\rangle} - 1\right) \approx \frac{1}{\theta_0}, \tag{A23}$$

since we are in the limit $\theta_0 \ll 1$. Note that keeping terms of higher order in $1/\theta_0$ in Eq. (A23) would not be consistent with the fact that the expansion is stopped at order 2 in Eq. (A22).

APPENDIX B: MUTUAL COULOMB INTERACTION ENERGY

We approximate the Coulomb interaction energy E_C by the expression given in Ref. [54] obtained by likening the fragments to homogeneously charged, spheroidal droplets with collinear symmetry axes coinciding with the fission direction:

$$E_C\left(Q_{20}^{(1)}, Q_{20}^{(2)}, D_{\mathrm{c.m.}}\right) = \frac{Z_1 Z_2 e^2}{D_{\mathrm{c.m.}}} S(x_1, x_2), \tag{B1}$$

where the eccentricity-like variable x_i is defined through its square as

$$x_i^2 = \frac{c_i^2 - a_i^2}{D_{\mathrm{c.m.}}^2}. \tag{B2}$$

In Eq. (B1), the dimensionless function S, expressing the departure from two spherical fragments, takes the form

$$\begin{aligned} S(x, y) \; = \; & \frac{3}{40}\left[\frac{1+11(x^2+y^2)}{x^2y^2} + P_x P_y\left(\frac{(1+x+y)^3}{x^3y^3}\right.\right. \\ & \times \ln(1+x+y)(1-3(x+y)+12xy \\ & \left.\left. -4(x^2+y^2))\right)\right]. \end{aligned} \tag{B3}$$

In this expression, $P_x[f(x)]$ represents the even part of the function $f(x)$:

$$P_x[f(x)] = \frac{f(x)+f(-x)}{2}. \tag{B4}$$

In Eq. (B2), c_i and a_i denote the semiaxes of the fragment i along the symmetry axis and in the perpendicular direction, respectively. They are related to the quadrupole moment $Q_{20}^{(i)}$ and the mean square radius $\langle\mathbf{r}^2\rangle^{(i)}$ in the spheroidal approximation neglecting the diffuseness effect:

$$Q_{20}^{(i)} = \tfrac{2}{5}A_i\left(c_i^2 - a_i^2\right), \tag{B5}$$

$$\langle\mathbf{r}^2\rangle^{(i)} = \tfrac{1}{5}\left(2a_i^2 + c_i^2\right), \tag{B6}$$

where A_i denotes the mass number of the fragment i. As can be seen in Eq. (B2), prolate shapes ($c_i > a_i$) lead to real x_i values, whereas x_i is purely imaginary for oblate shapes ($c_i < a_i$). As expected, we have $S(0, 0) = 1$ for two spheres.

When the deformation of at least one fragment is small, that is, when $|x| \leqslant x_{\max}$ and/or $|y| \leqslant y_{\max}$, we use a Taylor expansion. With threshold values $x_{\max}$ and $y_{\max}$ equal to 10^{-2}, for which the computation of E_C using Eq. (B3) does not pose any numerical problem, it is sufficient to include terms of order 2 at most. However, for completeness and possible uses with higher values of $x_{\max}$ and $y_{\max}$, we give expansions of $S(x, y)$ up to order 6:

$|x| \leqslant x_{\max}$ and $|y| > y_{\max}$:

$$\begin{aligned} S(x, y) \; = \; & \frac{3}{4y^3}\left[2y + (y^2-1)\ln\left(\frac{1+y}{1-y}\right)\right] \\ & \times\left(1 - \frac{x^2}{5(y^2-1)}\right) - \frac{x^4}{(y^2-1)^3} \\ & \times\left(\frac{3}{35} + \frac{(5+3y^2)x^2}{105(y^2-1)^2}\right). \end{aligned} \tag{B7}$$

$|x| > x_{\max}$ and $|y| \leqslant y_{\max}$: same as Eq. (B7) with x and y interchanged.

$|x| \leqslant x_{\max}$ and $|y| \leqslant y_{\max}$:

$$\begin{aligned} S(x, y) \; = \; & 1 + \frac{x^2+y^2}{5} + \frac{6}{25}x^2y^2 + \frac{3}{35}(x^4+y^4) \\ & + \frac{9}{35}x^2y^2(x^2+y^2) + \frac{x^6+y^6}{21}. \end{aligned} \tag{B8}$$

APPENDIX C: NUMERICAL ASPECTS

In this Appendix, we address the numerical issues that arise when calculating quantities of physical interest at scission. To set up the framework and make this Appendix self-contained, we briefly recall some considerations already mentioned in Sec. V. Our degrees of freedom are the center-of-mass distance $D_{\mathrm{c.m.}}$ and the fragment elongations expressed as their quadrupole moments $Q_{20}^{(1)}$ and $Q_{20}^{(2)}$. The relevant scission-configuration space $\mathcal{S}$ is therefore three-dimensional (3D). A scission configuration is characterized by three conditions:

$$\left|\frac{E_N}{E_C}\right| = \eta, \tag{C1}$$

$$E_{\mathrm{free}} \geqslant 0, \tag{C2}$$

and

$$d \geqslant 0, \tag{C3}$$

where E_N and E_C denote the nuclear and Coulomb interaction energies, respectively, E_{free} is the available energy at scission and d is the tip distance. The condition expressed by Eq. (C1) gives $D_{\mathrm{c.m.}}$ as a function of $Q_{20}^{(1)}$ and $Q_{20}^{(2)}$ (single-valued and smooth as shown in Fig. 4), whereas Eqs. (C1) and (C3) limit the set $\mathcal{S}_Q$ of possible values for $Q_{20}^{(1)}$ and $Q_{20}^{(2)}$ at scission. To these three conditions are added two limitations inherent to practical calculations:

$$\left(Q_{20}^{(i)}\right)_{\min} \leqslant Q_{20}^{(i)} \leqslant \left(Q_{20}^{(i)}\right)_{\max}, \tag{C4}$$

and

$$d \leqslant d_{\max}. \tag{C5}$$

Clearly Eq. (C4) introduces a truncation of $\mathcal{S}_Q$ that has to be limited to ranges of reasonable fragment shapes (rather close to the ground-state shapes). In contrast, Eq. (C5) is inconsequential when $d_{\max}$ is large enough (at least 6 fm here). Finally, let us recall in what kind of physically relevant quantities we are interested (called here "observables" even if they are not measurable).

We essentially want to calculate constrained averages of observables, that is, averaged over a subset of $\mathcal{S}$ corresponding to scission configurations having the same total excitation energy (TXE). We call $\mathcal{C}_{\text{TXE}}(E_x)$ the locus of points of $\mathcal{S}$ at which the function TXE$(D_{\text{c.m.}}, Q_{20}^{(1)}, Q_{20}^{(2)})$ takes a given value E_x. In general, this constraint makes the subset $\mathcal{C}_{\text{TXE}}(E_x)$ a non-simply-connected skew curve. Each simply connected piece noted $\mathcal{C}_{\text{TXE}}^{(i)}(E_x)$ and indexed by i can be represented by parametric equations of the form

$$\begin{cases} Q_{20}^{(1)} = f_i(s), \\ Q_{20}^{(2)} = g_i(s), \\ D_{\text{c.m.}} = h_i(s), \end{cases} \tag{C6}$$

where the curvilinear abscissa s along $\mathcal{C}_{\text{TXE}}(E_x)$ has been chosen as parameter. Since TXE is a continuous function of $D_{\text{c.m.}}$, $Q_{20}^{(1)}$, and $Q_{20}^{(2)}$, so are the one-variable functions f_i, g_i, and h_i in their respective domains. The constrained average $\overline{X}_{\text{TXE}}(E_x)$ of any observable X is defined as the average of X over the scission configurations along $\mathcal{C}_{\text{TXE}}(E_x)$:

$$\begin{aligned}\overline{X}_{\text{TXE}}(E_x) = \sum_{i=1}^{N_c} \int_{\mathcal{C}_{\text{TXE}}^{(i)}(E_x)} ds\, w(f_i(s), g_i(s), h_i(s)) \\ \times X(f_i(s), g_i(s), h_i(s)),\end{aligned} \tag{C7}$$

where $w(Q_{20}^{(1)}, Q_{20}^{(2)}, D_{\text{c.m.}})$ denotes the probability of reaching the scission configuration characterized by $Q_{20}^{(1)}, Q_{20}^{(2)}$, and $D_{\text{c.m.}}$. In Eq. (C7), the sum runs over the N_c simply connected pieces of $\mathcal{C}_{\text{TXE}}(E_x)$.

As discussed in Sec. VI, we represent the 3D curves $\mathcal{C}_{\text{TXE}}(E_x)$ by their projection on the $(Q_{20}^{(1)}, Q_{20}^{(2)})$ plane but the constrained averages are still calculated in the 3D space using Eq. (C7). From now on we call $\mathcal{C}_{\text{TXE}}$ the projection of the 3D curve, i.e., the iso-TXE contour level on the $(Q_{20}^{(1)}, Q_{20}^{(2)})$ plane.

To obtain one such contour, we first discretize the $Q_{20}^{(1)}$ axis and solve numerically the equation TXE$(Q_{20}^{(1)}, Q_{20}^{(2)})$ for $Q_{20}^{(2)}$. Then we repeat this step upon interchanging the role of the two fragment elongations. The reason for this is that the first step is not appropriate for finding solutions to the above equation when the tangent to the TXE contour becomes almost parallel to the $Q_{20}^{(2)}$ axis, and conversely for the second step. Once the solutions on the discretized $(Q_{20}^{(1)}, Q_{20}^{(2)})$ plane are found after the two steps, the corresponding points are connected with segmented lines of minimal length between two consecutive points. In practice, we have found that using a mesh size of 5 fm^2 gives complete, very smooth contours (see Fig. 5).

In fact, a particularly difficult problem is to design a reliable numerical algorithm to isolate the different pieces of $\mathcal{C}_{\text{TXE}}$. For a non-simply-connected contour, the above algorithm to connect scission points leads to large increases of the curvilinear abscissa between some consecutive points. In most practical cases, we have been able to detect these jumps by comparing the distance Δs between two consecutive points of the sequence approximating $\mathcal{C}_{\text{TXE}}$ with a critical value $\Delta s_{\max}$. When $\Delta s > \Delta s_{\max}$, we interpret the large increase as a jump from a point of one piece of $\mathcal{C}_{\text{TXE}}$ to a point of another piece. Empirically we have found that by choosing $\Delta s_{\max} = \sqrt{(\Delta x)^2 + (\Delta y)^2}$ with $\Delta x = \Delta y = 100$ fm^2, we can eliminate all the spurious jumps.

To close this Appendix, we indicate how we calculate the integral involved in Eq. (C7). For each complete TXE contour, in the sense defined in Sec. VII B, we approximate the integral by the trapezoidal rule along the segmented line representing the contour $\mathcal{C}_{\text{TXE}}$ but with the 3D Cartesian metric instead of the 2D one used to construct $\mathcal{C}_{\text{TXE}}$. It is safe here to do so because the third coordinate $D_{\text{c.m.}}$ is slowly varying with the other two. The resulting expression for the average of X for a given value of TXE, noted $\overline{X}$(TXE) for simplicity, takes the form

$$\overline{X}(\text{TXE}) \approx \frac{1}{2} \sum_{i=1}^{N_c} \sum_{k=1}^{n(i)-1} \Delta s_k \left(w_k X_k + w_{k+1} X_{k+1}\right), \tag{C8}$$

where $n(i)$ is the number of actual grid points making the subset i of $\mathcal{C}_{\text{TXE}}$. In Eq. (C8), Δs_k denotes the distance in the 3D space between the point P_k and the next one, P_{k+1}. Similarly, w_k and X_k are the values taken by the scission-configuration probability w and the observable X at point P_k, respectively. Note that the dependence on TXE in the right member of Eq. (C8) is hidden in the actual values of Δs, w, and X at the different points P_k belonging to the 3D curve.

---

[1] R. Vandenbosch and J. R. Huizenga, *Nuclear Fission* (Academic Press, New York, 1973), Ch. 13.

[2] D. de Frenne, in *The Nuclear Fission Process,* edited by C. Wagemans (CRC, Boca Raton, FL, 1991), Ch. 9.

[3] I. Ahmad and W. R. Phillips, Rep. Prog. Phys. **58**, 1415 (1995).

[4] I. N. Mikhailov and P. Quentin, Phys. Lett. **B462**, 7 (1999).

[5] H. R. Bowman and S. G. Thompson, in *Proceedings of the 2nd U.N. International Conference on Peaceful Uses of Atomic Energy* (United Nations, Geneva, 1958), Vol. 15, p. 212.

[6] A. Smith, P. Fields, A. Friedman, S. Cox, and R. Sjoblom, in *Proceedings of the 2nd U.N. International Conference on*

Peaceful Uses of Atomic Energy (United Nations, Geneva, 1958), Vol. 15, p. 392.

[7] M. M. Hoffman, Phys. Rev. **133**, B714 (1964).

[8] H. Maier-Leibnitz, P. Armbruster, and H. J. Specht, in *Proceedings of the IAEA Symposium on the Physics and Chemistry of Fission, Salzburg* (IAEA, Vienna, 1965), Vol. 2, p. 113.

[9] H. Nifenecker, C. Signarbieux, R. Babinet, and J. Poitou, *Proceedings of the 3rd IAEA Symposium on the Physics and Chemistry of Fission, Rochester, NY* (IAEA, Vienna, 1973), Vol. 2, p. 117.

[10] J. R. Huizenga and R. Vandenbosch, Phys. Rev. **120**, 1305 (1960); R. Vandenbosch and J. R. Huizenga, Phys. Rev. **120**, 1313 (1960).

[11] J. B. Wilhelmy, E. Cheifetz, R. C. Jared, S. G. Thompson, H. R. Bowman, and J. O. Rasmussen, Phys. Rev. C **5**, 2041 (1972).

[12] P. Glässel, R. Schmid-Fabian, D. Schwalm, D. Habs, and H. U. v. Helmolt, Nucl. Phys. **A502**, 315c (1989).

[13] G. S. Popeko *et al.*, in *Proceedings of the 2nd International Conference on Fission and Properties of Neutron-Rich Nuclei* (World Scientific, Singapore, 1998), p. 645; G. M. Ter-Akopian *et al.*, *Proceedings of the 3rd International Conference on Fission and Properties of Neutron-Rich Nuclei* (World Scientific, Singapore, 1999), p. 98.

[14] G. M. Ter-Akopian, J. H. Hamilton, Yu. Ts. Oganessian, J. Kormicki, G. S. Popeko, A. V. Daniel, A. V. Ramayya, Q. Lu, K. Butler-Moore, W. C. Ma, J. K. Deng, D. Shi, J. Kliman, V. Polhorsky, M. Morhac, W. Greiner, A. Sandelescu, J. D. Cole, R. Aryaeinejad, N. R. Johnson, I. Y. Lee, and F. K. McGowan, Phys. Rev. Lett. **73**, 1477 (1994).

[15] G. M. Ter-Akopian, J. H. Hamilton, Yu. Ts. Oganessian, A. V. Daniel, J. Kormicki, A. V. Ramayya, G. S. Popeko, B. R. S. Babu, Q.-H. Lu, K. Butler-Moore, W.-C. Ma, S. Ćwiok, W. Nazarewicz, J. K. Deng, D. Shi, J. Kliman, M. Morhac, J. D. Cole, R. Aryaeinejad, N. R. Johnson, I. Y. Lee, F. K. McGowan, and J. X. Saladin, Phys. Rev. Lett. **77**, 32 (1996).

[16] J. H. Hamilton, A. V. Ramayya, J. Kormicki, W.-C. Ma, Q. Lu, D. Shi, J. K. Deng, S. J. Zhu, A. Sandulescu, W. Greiner, G. M. Ter-Akopian, Yu. Ts. Oganessian, G. S. Popeko, A. V. Daniel, J. Kliman, V. Polhorsky, M. Morhac, J. D. Cole, R. Aryaeinejad, I. Y. Lee, N. R. Johnson, and F. K. McGowan, J. Phys. G **20**, L85 (1994).

[17] S. A. E. Johansson, Nucl. Phys. **60**, 378 (1964).

[18] J. S. Fraser and J. C. D. Milton, Phys. Rev. **93**, 818 (1964); J. Terrell, in *Proceedings of the IAEA Symposium on the Physics and Chemistry of Fission, Salzburg* (IAEA, Vienna, 1965), Vol. 2, p. 3.

[19] E. K. Hulet, J. F. Wild, R. J. Dougan, R. W. Lougheed, J. H. Landrum, A. D. Dougan, M. Schädel, R. L. Hahn, P. A. Baisden, C. M. Henderson, R. J. Dupzyk, K. Sümmerer, and G. R. Bethune, Phys. Rev. Lett. **56**, 313 (1986).

[20] J. O. Newton, Prog. Nucl. Phys. **4**, 234 (1955); J. A. Wheeler, *Niels Bohr and the Development of Physics* (W. Pauli ed., Pergamon, Oxford, 1955), p. 163.

[21] P. A. Russo, R. Vandenbosch, M. Mehta, J. R. Tesmer, and K. L. Wolf, Phys. Rev. C **3**, 1595 (1971).

[22] F. Gönnenwein, I. Tsekanovich, and V. Rubchenya, Int. Mod. Phys. E **16**, 410 (2007).

[23] J. L. Durell, in *Proceedings of the 3rd International Conference on Dynamical Aspects of Nuclear Fission,* edited by J. Kliman and B. I. Pustylnic (World Scientific, Singapore, 1996), p. 270.

[24] V. M. Strutinsky, Zh. Eksp. Teor. Fiz. **37**, 861 (1959) [Sov. Phys.-JETP **10**, 613 (1960)].

[25] M. Zielinska-Pfabé and K. Dietrich, Phys. Lett. **B49**, 123 (1974).

[26] Ş. Mişicu, A. Sandulescu, G. M. Ter-Akopian, and W. Greiner, Phys. Rev. C **60**, 034613 (1999).

[27] I. N. Mikhailov, P. Quentin, and Ch. Briançon, Yad. Fiz. **64**, 1185 (2001); Phys. At. Nucl. **64**, 1110 (2001).

[28] J. R. Nix and W. J. Swiatecki, Nucl. Phys. **71**, 1 (1965).

[29] L. G. Moretto, G. F. Peaslee, and G. J. Wozniak, Nucl. Phys. **A502**, 453c (1989).

[30] J. O. Rasmussen, W. Nörenberg, and H. J. Mang, Nucl. Phys. **A136**, 465 (1969).

[31] P. O. Hess and W. Greiner, II Nuovo Cimento **83A**, 76 (1984).

[32] N. V. Antonenko, E. A. Cherepanov, A. K. Nasirov, V. P. Permjakov, and V. V. Volkov, Phys. Rev. C **51**, 2635 (1995).

[33] Ş. Mişicu, A. Sandulescu, and W. Greiner, Mod. Phys. Lett. A **12**, 1343 (1997).

[34] T. M. Shneidman, G. G. Adamian, N. V. Antonenko, S. P. Ivanova, R. V. Jolos, and W. Scheid, Phys. Rev. C **65**, 064302 (2002).

[35] L. Bonneau, Phys. Rev. C **74**, 014301 (2006).

[36] H. Goutte, J.-F. Berger, and D. Gogny, Int. J. Mod. Phys. E **15**, 292 (2006).

[37] M. Warda, J. L. Egido, L. M. Robledo, and K. Pomorski, Phys. Rev. C **66**, 014310 (2002).

[38] G. G. Adamian, N. V. Antonenko, R. V. Jolos, S. P. Ivanova, and O. I. Melnikova, Int. J. Mod. Phys. E **5**, 191 (1996).

[39] G. G. Adamian, N. V. Antonenko, S. P. Ivanova, and W. Scheid, Nucl. Phys. **A646**, 29 (1999).

[40] F. Gönnenwein and B. Börsig, Nucl. Phys. **A530**, 27 (1991).

[41] F. Pleasanton, R. L. Ferguson, and H. W. Schmitt, Phys. Rev. C **6**, 1023 (1972).

[42] Yu. N. Kopach, P. Singer, M. Mutterer, M. Klemens, A. Hotzel, D. Schwalm, P. Thirolf, M. Hesse, and F. Gönnenwein, Phys. Rev. Lett. **82**, 303 (1999).

[43] S. Frauendorf, Z. Phys. A **358**, 163 (1997).

[44] I. N. Mikhailov, P. Quentin, and D. Samsoen, Nucl. Phys. **A627**, 259 (1997).

[45] R. E. Peierls and J. Yoccoz, Proc. Phys. Soc. London Sect. A **70**, 381 (1957).

[46] N. Lo Iudice and F. Palumbo, Phys. Rev. Lett. **41**, 1532 (1978).

[47] H. J. Krappe, J. R. Nix, and A. J. Sierk, Phys. Rev. C **20**, 992 (1979).

[48] K. Pomorski and K. Dietrich, Z. Phys. A **295**, 355 (1980).

[49] P. Möller, J. R. Nix, W. D. Myers, and W. J. Swiatecki, At. Data Nucl. Data Tables **59**, 185 (1995).

[50] L. Bonneau, P. Quentin, and D. Samsœn, Eur. Phys. J. A **21**, 391 (2004).

[51] L. Bonneau and P. Quentin, Phys. Rev. C **72**, 014311 (2005).

[52] L. Bonneau and P. Quentin, in *Proceedings of the 3rd International Workshop on Nuclear Fission and Fission-Product Spectroscopy,* edited by H. Goutte, H. Faust, G. Fioni, and D. Goutte (AIP, New York, 2005), p. 77.

[53] A. J. Sierk, Phys. Rev. C **33**, 2039 (1986).

[54] P. Quentin, J. Phys. (Paris) **30**, 497 (1969).

[55] Ş. Mişicu and P. Quentin, Eur. Phys. J. A **6**, 399 (1999).

[56] B. D. Wilkins, E. P. Steinberg, and R. R. Chasman, Phys. Rev. C **14**, 1832 (1976).

[57] D. G. Madland and J. R. Nix, Nucl. Phys. **A476**, 1 (1988).

[58] J. Dobaczewski, P. Magierski, W. Nazarewicz, W. Satula, and Z. Szymański, Phys. Rev. C **63**, 024308 (2001).

[59] S. J. Krieger, P. Bonche, H. Flocard, P. Quentin, and M. S. Weiss, Nucl. Phys. **A517**, 275 (1990).
[60] H. Flocard, P. Quentin, A. K. Kerman, and D. Vautherin, Nucl. Phys. **A203**, 433 (1973).
[61] D. W. Sprung, S. G. Lie, M. Vallières, and P. Quentin, Nucl. Phys. **A326**, 37 (1979).
[62] M. Born and R. Oppenheimer, Ann. Phys. (Leipzig) **84**, 457 (1927).
[63] J. W. Negele, S. E. Koonin, P. Möller, J. R. Nix, and A. J. Sierk, Phys. Rev. C **17**, 1098 (1978).
[64] Å. Bohr and B. R. Mottelson, in *Nuclear Structure* (World Scientific, Singapore, 1998), Vol. 1, p. 159.
[65] F. Gönnenwein, in *The Nuclear Fission Process,* edited by C. Wagemans (CRC, Boca Raton, FL, 1991), Ch. 8.
[66] F. Rejmund, A. V. Ignatyuk, A. R. Junghans, and K.-H. Schmidt, Nucl. Phys. **A678**, 215 (2000).
[67] J. R. Huizenga and R. Vandenbosch, in *Nuclear Reactions,* edited by P. M. Endt, M. Demeur, and P. B. Smith (North-Holland, Amsterdam, 1959), Vol. 2.
[68] J.-F. Berger, M. Girod, and D. Gogny, Nucl. Phys. **A428**, 23c (1989).
[69] M. Abramowitz and I. Stegun, *Handbook of Mathematical Functions* (Dover, New York, 1972).